

ABSTRACT

Title of Thesis: BEHAVIOR AND ANALYSIS OF AN INSTRUMENTED
SLAB BRIDGE

Sungki Jeong, Master of Science in Civil Engineering 2009

Thesis Directed By: Professor Chung C. Fu
Department of Civil and Environmental Engineering

Because of quick construction and cost effectiveness, adjacent precast, prestressed box girder bridges have been used nowadays more often for short-span bridges, and the standardization of this modular bridge is highly desired. Maryland intends to revise its current practice of using tie-rods for the transverse post-tensioning in slab bridge design. The new design of using high strength rods will provide a more tightly integrated modular slab bridge system with higher post-tensioning forces. With the new design, the Maryland State Highway Administration is highly interested in the performance of the new design, especially compared with the old design. This thesis presents the procedure of test, live load test results and analysis results in association with the finite-element model simulated in a newly-built bridge.

BEHAVIOR AND ANALYSIS OF AN INSTRUMENTED SLAB BRIDGE

By

Sungki Jeong

Thesis submitted to the Faculty of the Graduate School of the
University of Maryland, College Park, in partial fulfillment
of the requirements for the degree of
[Master of Science]
[2009]

Advisory Committee:
Professor [Chung C. Fu], Chair
[Professor M. Sherif Aggour]
[Professor Amde M. Amde]

© Copyright by
Sungki Jeong
2009

Acknowledgements

This work was sponsored by the FHWA of US DOT and Maryland State DOT through FHWA's Innovative Bridge Research and Construction (IBRC) program. Thanks also are due to Maryland DOT: Jeff Robert for the coordination, Jason Pollock, project engineer of the project, Glenn Vaughan, Chief of the Bridge Design Division, and Jock Freedman, Director of the Office of Bridge Development for their logistic and administrative support.

Table of Contents

ACKNOWLEDGEMENTS	ii
TABLE OF CONTENTS	iii
LIST OF FIGURES	iv
LIST OF TABLES	vi
1. INTRODUCTION	1
2. FIELD LOAD TEST PROCEDURE	3
2.1 DESCRIPTION OF THE TEST BRIDGE	3
2.2 INSTRUMENTATION PLAN	7
2.2.1 Gage locations	7
2.2.2 Instrumentation	8
2.2.3 Resistance Strain in Gages	9
2.2.4 BDI Strain Transducer	10
2.2.5 Data Acquisition System	12
2.2.6 CR5000	12
2.2.7 Dell laptop computer w/PC9000.....	13
2.2.8 AM16/32 Relay Multiplexers	14
2.3 LAB TEST.....	14
2.4 LIVE LOAD TESTS.....	17
2.4.1 Installation and Field Setup	17
2.4.2 Test Vehicle	20
2.4.3 Result of Live Load Test.....	22
3. MODELING	25
3.1 SECTIONS OF ANSYS BRIDGE MODEL	25
3.2 MATERIAL PROPERTY	26
3.3 MODELING METHOD.....	27
3.4 LOADING AND BOUNDARY CONDITION	27
3.5 RESULT OF FINITE ELEMENT ANALYSIS	28
4. SUMMARY OF RESULT	30
5. PARAMETRIC STUDY	33
5.1 INVESTIGATION OF MODEL.....	33
5.2 SHEAR KEY INVESTIGATION	37
5.3 SEQUENCE OF CONSTRUCTION OF SHEAR KEY	40
5.4 PARAMETRIC STUDY ON VARYING POST-TENSIONING FORCES OF THE TESTED 35'-SPAN BRIDGE	41
5.5 PARAMETRIC STUDY ON BRIDGES OF OTHER SPAN LENGTHS	42
6. CONCLUSION	47
REFERENCES	48

List of Figures

Figure 1 - Structure No. 0901100 Wallace Creek Bridge (Old).....	4
Figure 2 - Structure No. 0901100 Wallace Creek Bridge (New)	4
Figure 3 - Structure No. 0901100 Wallace Creek Bridge (Plan View)	5
Figure 4 - Structure No. 0901100 Wallace Creek Bridge (Elevation View).....	5
Figure 5 - Structure No. 0901100 Wallace Creek Bridge (Slab Detail at Midspan)	6
Figure 6 - Structure No. 0901100 Wallace Creek Bridge (Slab Detail at End).....	6
Figure 7 - Map of Sensor Locations	8
Figure 8 - VISHAY N2A-06-20CBW-350 Principle & Property	10
Figure 9 - BDI strain gage Dimension.....	11
Figure 10 - Installed BDI strain gage.....	11
Figure 11 - Data Acquisition Diagram.....	12
Figure 12 - Campbell Science CR5000 Data Logger	13
Figure 13 - AM16/32 Relay Multiplexers	14
Figure 14 - Sample Testing Concrete Blocks	15
Figure 15 - Vishay Strain Gage Flexure Testing	16
Figure 16 - BDI Strain Transducer Flexure Testing.....	16
Figure 17 - INSTRON Sample Result	17
Figure 18 - Paths of Test Truck (Position of Left Wheel of Test Truck)	19
Figure 19 - Data Acquisition System during Monitoring	19
Figure 20 - Summary of Live Load Test Set-Up	20
Figure 21 - Testing Vehicle	21
Figure 22 - Vehicle Load Configuration.....	21
Figure 23 - BDI Gages Scrawling on Beam2	23
Figure 24 - Types of Sections in FEM Bridge Model	26
Figure 25 - Isometric View of the Bridge Mode.....	28
Figure 26 - Summary of Test 1	30
Figure 27 - Summary of Test 2.....	31
Figure 28 - Longitudinal Strain Distribution of Bridge Model.....	32
Figure 29 - Longitudinal Strain Distribution of Bridge Model.....	33

Figure 30 - Concrete Beam Penetration-1	35
Figure 31 - Concrete Beam Penetration-2	35
Figure 32 - CONTA174 Geometry	36
Figure 33 - TARGE170 Geometry	36
Figure 34 - Contact Element.....	37
Figure 35 - Transverse Stress Distribution Diagram of Shear Key	39
Figure 36 – Lateral Post-Tensioning Rod Detail	40
Figure 37 – Shear Key Detail.....	40
Figure 38 - Displacement of Middle Span.....	41
Figure 39 - Microstrain under Post-Tension.....	42
Figure 40 – Cross Section of Analyzing Bridge (35', 40', 45', 50', and 55' Span)...	43
Figure 41 – Finite Element Model of Bridge as Maryland Code of Practice	44
Figure 42 – Stabilization of Deflection on 35ft Span Bridge	44
Figure 43 - Stabilization of Deflection on 40ft Span Bridge.....	45
Figure 44 - Stabilization of Deflection on 45ft Span Bridge.....	45
Figure 45 - Stabilization of Deflection on 50ft Span Bridge.....	45
Figure 46 - Stabilization of Deflection on 55ft Span Bridge.....	46

List of Tables

Table 1 - Location and Number of Sensors	8
Table 2 - Set of Post-Tensioning Force	18
Table 3 – Summary of Maximum Strain in Set 1	22
Table 4 - Summary of Maximum Strain in Set 2.....	22
Table 5 - Material Property.....	26
Table 6 - Finite Element Model Result - Beam2	29
Table 7 - Finite Element Model – Beam4.....	29
Table 8 - Uncracked Case of Shear Key	34
Table 9 - Cracked Case of Shear Key.....	34
Table 10 - Current Maryland Code of Practice.....	41
Table 11 - Other States’ Practices of the Transverse Post-tensioning.....	43
Table 12 - Transverse Post-Tension Required in Stabilizing Deflection of Beams ...	46

1. INTRODUCTION

Because of their quick construction and cost effectiveness, adjacent precast, prestressed multi-girder bridges have been used nowadays more often for short-spans. During its service years, many attempts at making more durable and robust adjacent precast, prestressed multi-girder bridges were made to prevent the bridges' typical deteriorations such as shear key failure, chloride's penetration into concrete deck, freeze-thaw damage, overlay cracking and so on. One of the attempts to fortify a bridge is to increase the level of post-tensioning forces that contribute to the bridge behaving monolithically; it will eventually alleviate the possibility of cracking on the bridge deck and shear key. Acknowledging the increase of the post-tensioning force is necessary and useful for facilitating better service of the bridge. In-depth investigation with field assessment of a bridge's real behavior will gain understanding of precast and prestressed multi-girder bridges' behavior.

The Maryland State Highway Administration (MD-SHA) has been adopting adjacent precast, prestressed multi-girder bridges as part of a continuous effort to minimize disruption to the traffic flow during construction. Opportunely, the bridge (Structure No. 0901100 in Maryland Bridge Inventory), located on the eastern shore of Maryland carrying Hooper's Island Road over Wallace Creek in Dorchester County, is being newly constructed. Since the current Maryland code of practice in design for this specific bridge now is proposed to be revised into a new design with higher post-tensioning forces, MD-SHA intends to validate the modification of its current code of practice in using tie-rods for the higher transverse post-tensioning force in slab bridge design. The new design of using higher post-tensioned rods will provide a further tightly integrated modular slab bridge system. Therefore, with the new design, the Maryland State Highway Administration has a great interest in the performance of the new design, especially compared with the old design.

In general, a post-tensioning system in a bridge provides structural integrity between the adjacent concrete girders in cooperation with the shear key because of higher ultimate strength due to the bond generated between the strands and concrete. In addition, it allows the strength of tendons to be adjustable according to the very

specific design specification. According to the study by the Bridge Engineering Software and Technology (BEST) Center regarding the impact of the transverse post-tensioning force required in prestressed concrete slabs, recommendations on modifying the MD SHA's standard details were made to defuse the overlay cracking problems. For a bridge span less than 40 feet, suggestions were made for MD SHA to modify the current practice of 30 kips post-tensioning force to 70 kips. (BEST center 2006) Since the evaluation of post-tensioned prestressed bridges with recommended forces has not been performed, there is a necessity for an in-depth study of bridge behavior under recommended post-tension forces. In addition, the tests in this paper have been implemented to analyze the post-tension effects of 30 kips and 80 kips.

Wallace Bridge was implemented to accomplish the primary purpose of observing short-term live load deck behaviors under the different transverse post-tensioning forces. Strain gages were used to measure strain under the two different post-tensioned forces, 30 kips and 80 kips. To meet this objective, a detailed instrumentation plan was produced to determine general and specific gage location.

2. FIELD LOAD TEST PROCEDURE

2.1 Description of the Test Bridge

The test bridge (Structure No. 0901100) is located on the eastern shore of Maryland carrying Hooper's Island Road over Wallace Creek in Dorchester County. The bridge has a single span, integral abutment structure built in 2008. The bridge consists of eleven adjacent 3'-0" wide x 1'-3" high x 36'-0" long prestressed concrete beams and an average 5.25" thick composite concrete deck. On each side of exterior concrete girder, curbs and guardrails are located.

All eleven concrete beams were respectively prestressed to have a strength of $f'_c = 7,000$ psi and a strength $f'_{ci} = 5,800$ psi at the transfer of prestress. Girders are integrated with a shear key along the full longitudinal direction and transversely post-tensioned at about the one-third points of the bridge span from both sides. With a total of 4 bars, each transverse post-tensioning bar integrates 6 concrete beams respectively. The ratings of the bridge are based on load factor design (LFD) utilizing HS-20 loading. The inventory and operating ratings of the bridge are LFD inventory HS-48 tons (96 kips) LFD operating HS-80 tons (160 kips). The test is performed before the bridge is opened to the traffic. The annual average daily traffic was 640 vehicles in 2004. (Construction Plan 0901100)

Because the old bridge experienced severe scour problems, SHA decided to replace the old, temporary bridge with a new bridge. According to the inspection report by SHA, the bridge is located at a tidal waterway and experiences a seasonal scour. (Structure Number 0901100) In addition, due to the partial structure left under the bridge, four corners of the bridge have been scoured. Photos and plans of the old and new bridges are shown in Figure 1 and Figure 2 respectively, and the new bridge beam sections are shown in Figure 3, Figure 4, Figure 5 and Figure 6.



Figure 1 - Structure No. 0901100 Wallace Creek Bridge (Old)



Figure 2 - Structure No. 0901100 Wallace Creek Bridge (New)

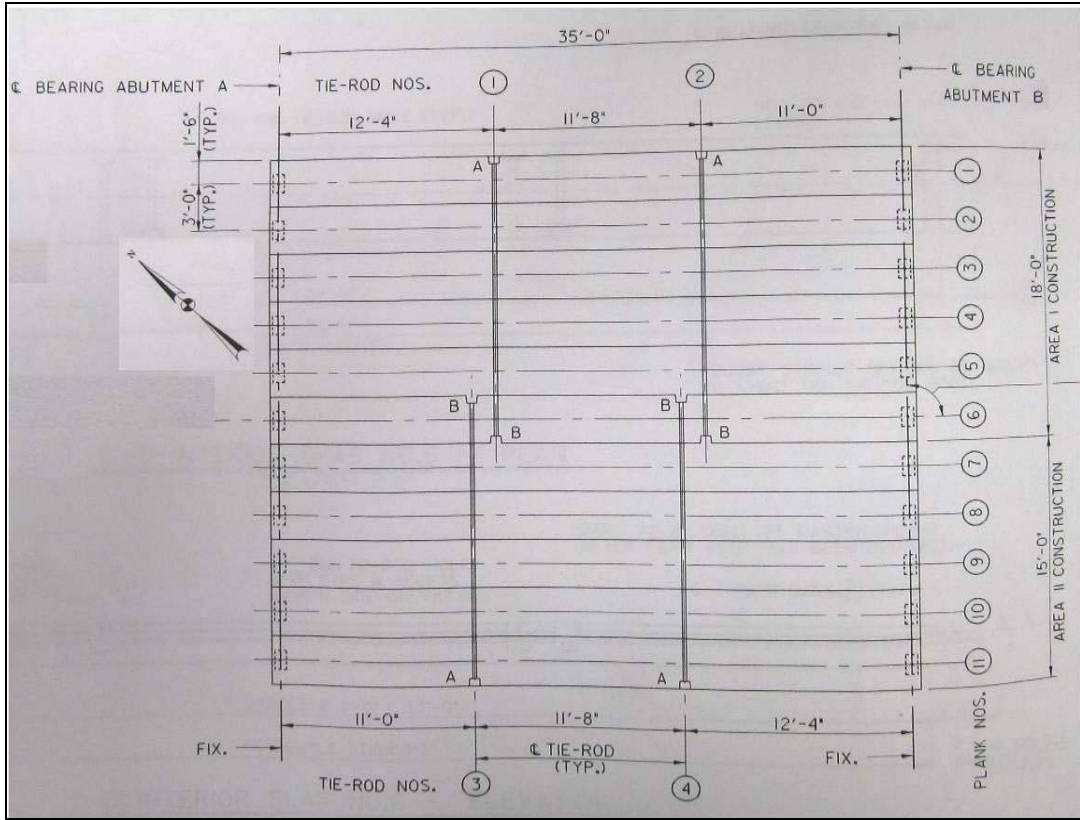


Figure 3 - Structure No. 0901100 Wallace Creek Bridge (Plan View)

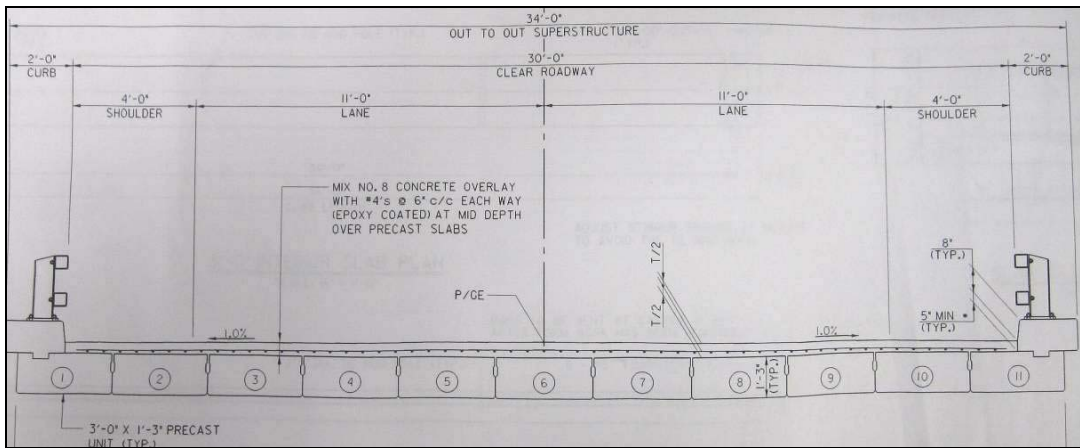


Figure 4 - Structure No. 0901100 Wallace Creek Bridge (Elevation View)

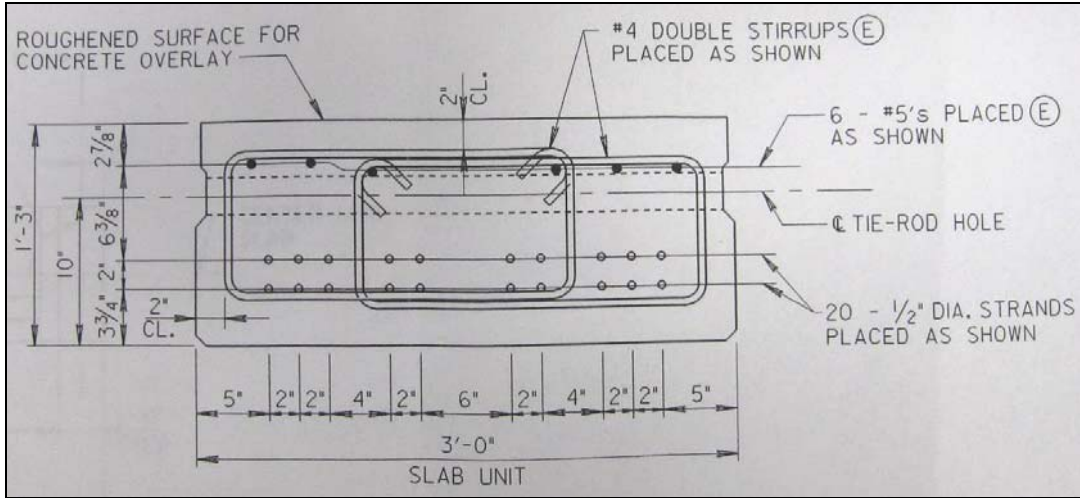


Figure 5 - Structure No. 0901100 Wallace Creek Bridge (Slab Detail at Midspan)

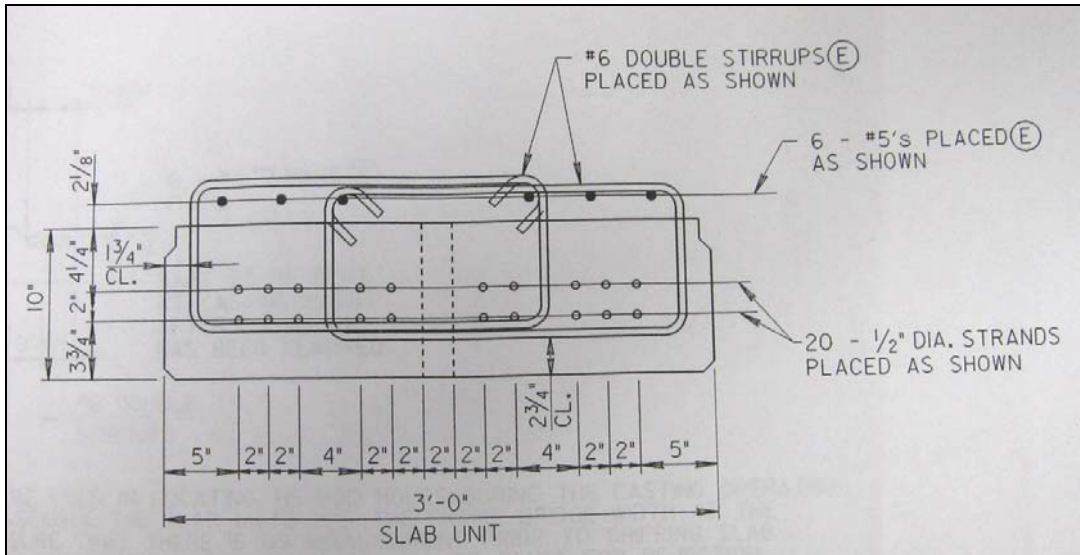


Figure 6 - Structure No. 0901100 Wallace Creek Bridge (Slab Detail at End)

2.2 Instrumentation Plan

Wallace Bridge was implemented to accomplish the primary purpose of observing short-term live load deck behaviors under different transverse post-tensioning forces. For monitoring separate strains under the bridge, two different strain sensors were used. To meet this objective, a detailed instrumentation plan was produced to determine general and specific gage locations. The instrumentation and data acquisition systems were chosen based on durability (suitable for long-term Structural Health Monitoring), reliability (data accuracy and reputation in the S Structural Health Monitoring industry) and compatibility (use in many devices and reusable in the future). The following will be introduced to describe details.

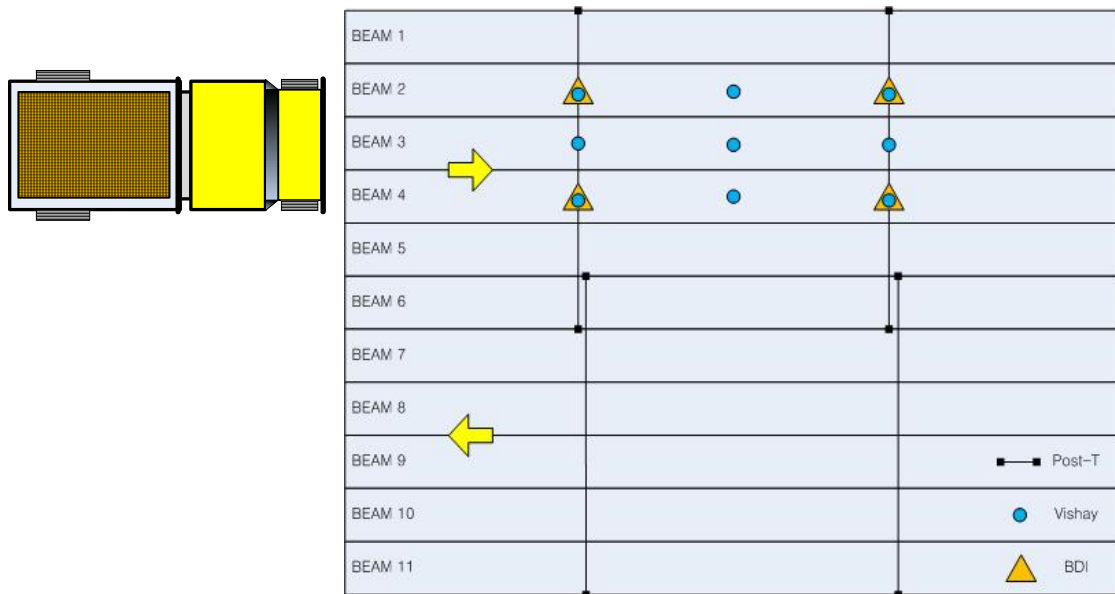
- 1) Gage locations
- 2) Instrumentation
- 3) Data acquisition system and setup
- 4) Components installation and assembly.

2.2.1 Gage locations

Locations of the sensors were selected mainly based on the targeted strain positions where the transverse post-tension rods are installed. Therefore, four BDI transducers and four Vishay sensors were installed on the bottom surface of concrete slab where the post-tension rods were located. All other locations were selected to obtain the most closely-related data and to characterize bridge behavior due to controlled variable, post-tension forces. In addition, gage locations were selected to investigate the interaction between the concrete girders and shear keys. See Figure 7 for detail of locations. Two BDI transducers were installed under the location of the post-tensioned rod in beam 2. And, two more BDI Transducers were installed under the location of the post-tensioned rod in beam 4. Additionally, 3 Vishay strain gauges per each beam were installed on beams 2 through 4 for comparison purposes. All locations have gages placed on the bottom surface of the concrete girders. The schematic of sensor locations is also shown in the Figure 7.

	BDI	VISHAY
BEAM 2	2	3
BEAM 3	0	3
BEAM 4	2	3

Table 1 - Location and Number of Sensors



Generally, these settings were preferred to investigate:

- Effects of the post-tensioning rod
- Difference of strain under the different post-tensioning force
- Load distribution on the girder
- Characteristics of strain data
- Global bending
- Effect of shear key
- Local deck behavior

2.2.2 Instrumentation

For instrumentation, two types of strain gages were used. Both gages were installed underneath the designated concrete girders. Vishay strain gages were soldered before installation and ready to attach. BDI (Bridge Diagnostics, Inc.) gages using vibrating wire were also prefabricated in advance of the live load test. These two types of gages were connected to CR5000, the data logger. Using the lead wires, the connections between all strain gages and the data logger were completed on

November 20, 2008 on the same day as the field test. All sensors were connected to the data logger correctly and their connections were checked by their specific resistance values using the multi-meter. Access to the underside of the bridge was enabled by using a float. Maryland State Highway provided all access, maintenance of traffic, and the loaded testing vehicle.

2.2.3 Resistance Strain in Gages

All local strain data by live load test was recorded directly to the data logger. These strain gages were bonded directly to the bottom surface of the concrete girders using cyanoacrylate (the instant adhesive). Gage installation was done by three research assistants from the University of Maryland, College Park. One of the two types of gages used, the Vishay strain gage, is made of a thin foil of Constantan (Copper-Nickel alloy) gage with laminated and polyimide-film backing. (Vishay 2008) Its metallic foil has an original resistance of $350.0 \pm 0.2\%$ (OHMs) and is designed for concrete and strain integration on large specimens. When the truck load is applied to the concrete girder, this default electrical resistance will change due to the foil's deformation in length. Because the changes are especially quite small, they are generally detected using a special circuit arrangement called a Wheatstone bridge. Figure 8 shows the gage's dimension and a basic principle. (Strain Gage, Wikipedia 2009)

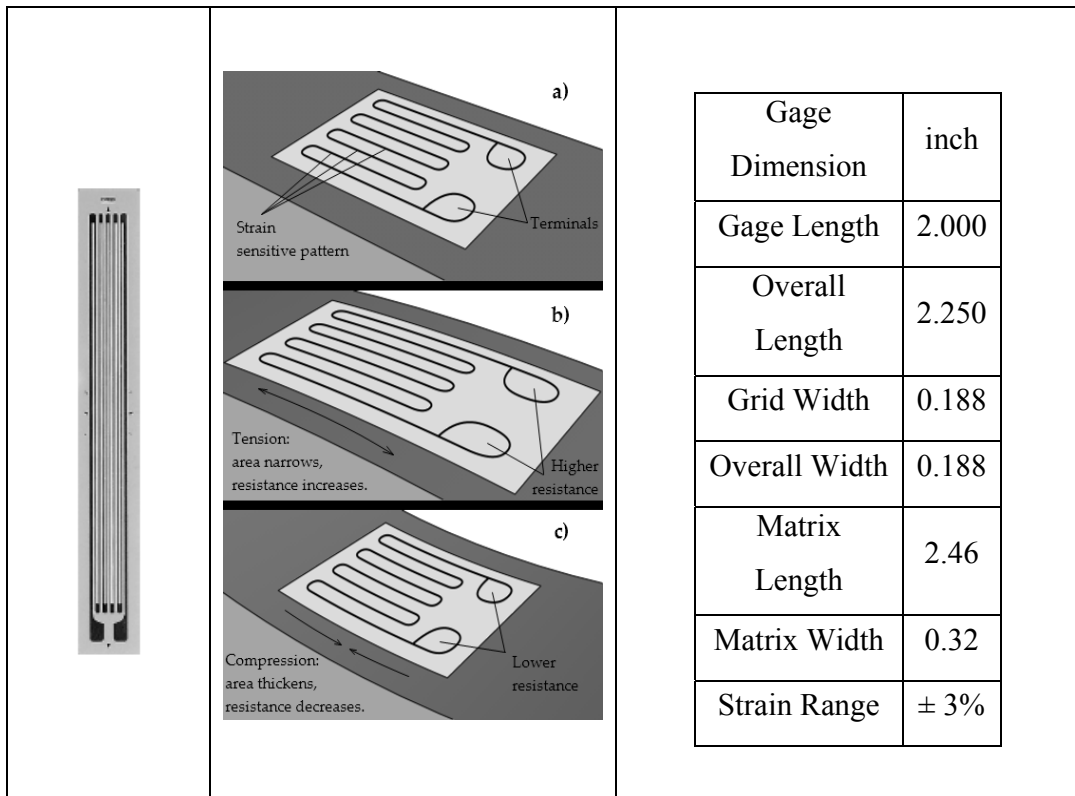


Figure 8 - VISHAY N2A-06-20CBW-350 Principle & Property

2.2.4 BDI Strain Transducer

For the live load test, Bridge Diagnostics, Inc (BDI) strain transducers were also used. It is designed to measure strain on bridges, buildings, cranes, and other civil structures and can be installed within minutes on steel, concrete, timber, and FRP members. Before installation, BDI transducers were first assembled with their extensions made of aluminum. They were then attached on the bottom of the concrete girders. Each BDI transducer has an effective gage length of 3.0 inch with 10 ft standard cable. During the live load test, averaging the strain over a longer gage length of 15 inch was used. Its strain range can reach up to $\pm 2000 \mu\epsilon$ with an accuracy of $\pm 2\%$. (Bridge Diagnostics, Inc. 2009) In addition, the resistance is measured at 350Ω . Figure 9 shows the dimension of a BDI transducer and Figure 10 shows one installed.

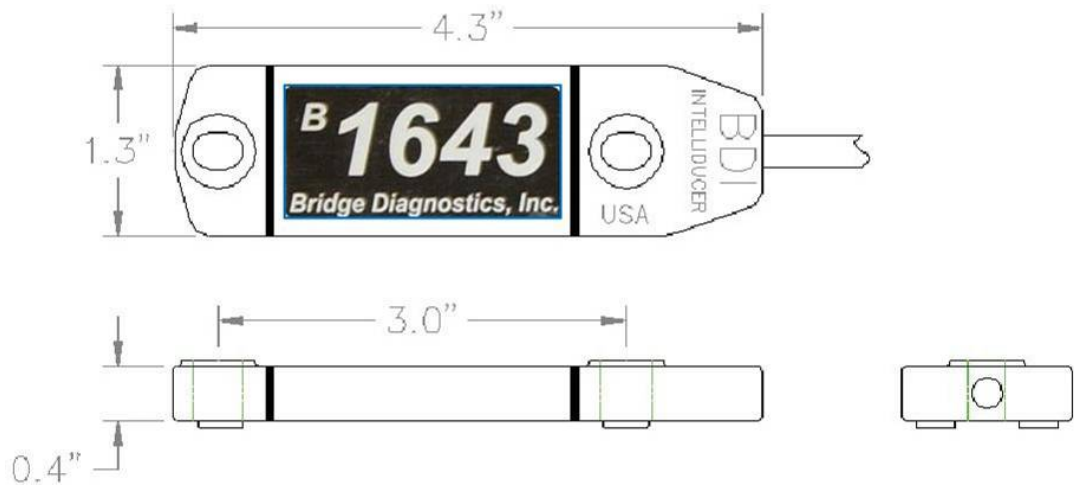


Figure 9 - BDI strain gage Dimension

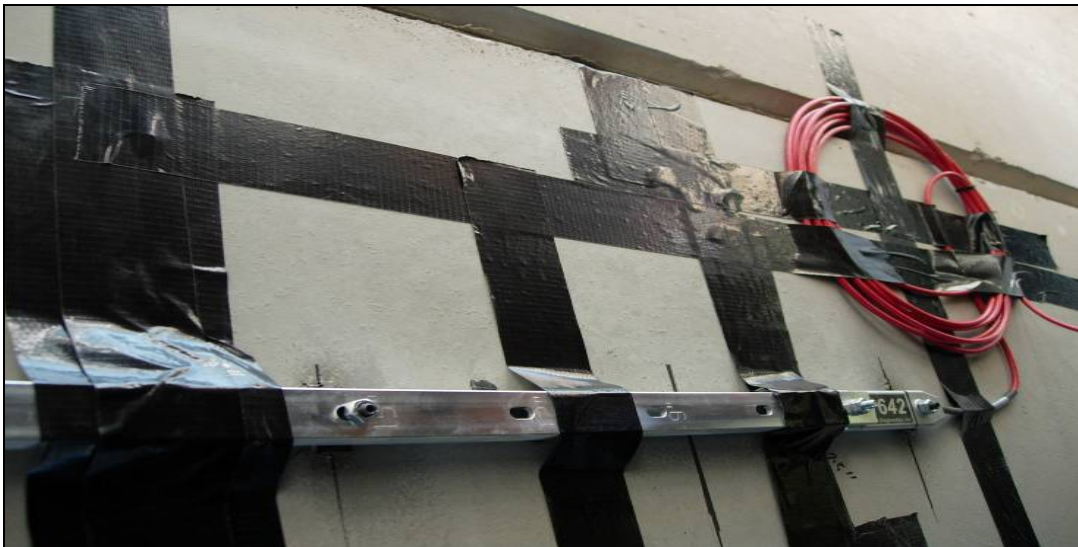


Figure 10 - Installed BDI strain gage

It is noted that west-bound bridge beams named as Beam 1 through Beam 6 with the original and recommended prestressing forces was instrumented. In addition, the data due to vehicular load was recorded and compared. All the sensor installation was done on the underside of the bridge beams. Since the bridge is over water, the float was used during installation.

2.2.5 Data Acquisition System

During the live load test, the CR5000 Measurement & Control System, Dell laptop computer and AM16/32 Relay Multiplexers was employed. For CR5000, main power source was supplied through the generator. Figure 11 shows a network of data acquisition systems and details of each device will be introduced.

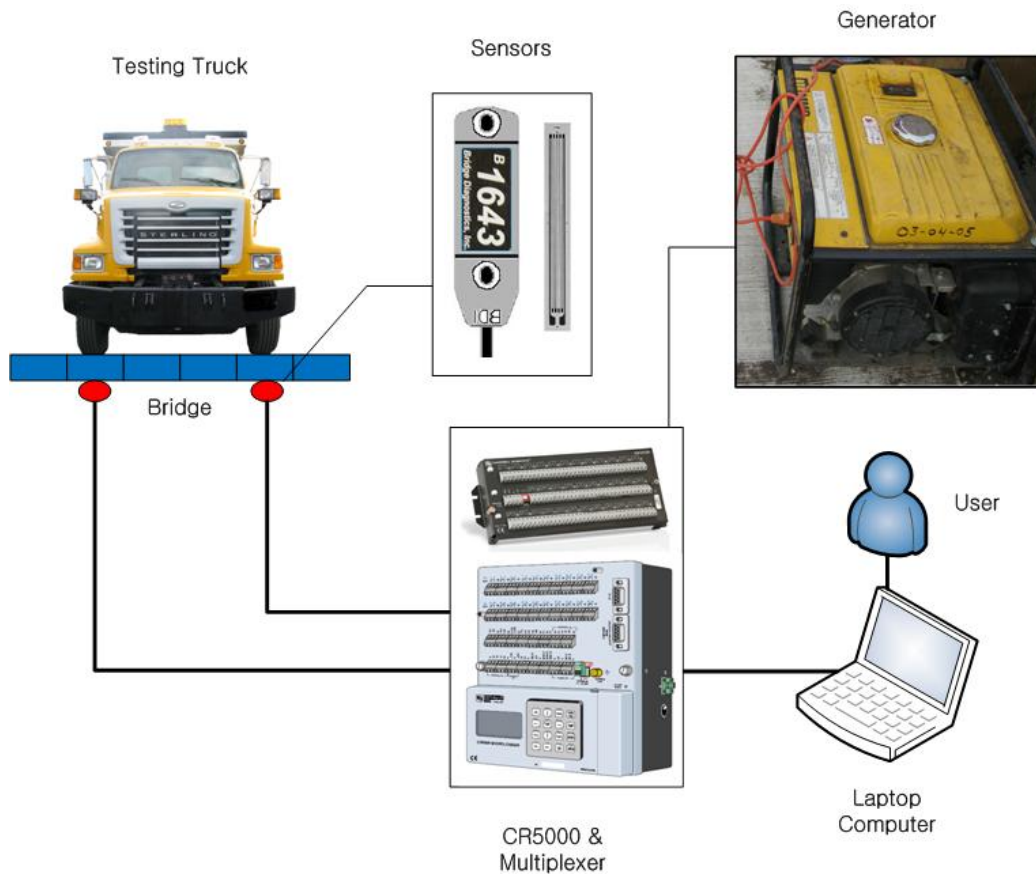


Figure 11 - Data Acquisition Diagram

2.2.6 CR5000

The CR5000 Measurement & Control System manufactured by Campbell Scientific, Inc. is a self-contained, low power, rugged data logger. It offers accurate measurement capabilities in a battery-operated package. For its components, CR5000 includes CPU, keyboard display, power supply, and analog and digital inputs and outputs. In terms of monitoring capability, CR5000 can provide maximum the average rate of successful message delivery over a communication channel of 5 kHz:

it takes measurements at a rate of up to 5,000 samples/second with 16-bit resolution. The on-board, BASIC-like programming language includes data processing and analysis routines. PC9000 Software provides program generation and editing, data retrieval, and real-time monitoring. Standard operating range is -77°F to +122°F with an optional extended range of -104°F to +185°F. (CR5000 Campbell Scientific, Inc. 2006) The on-board operating system contains measurement, processing, and output instructions for programming the data logger. In addition, CR5000 can be used for further research purposes in the future such as long term monitoring.



Figure 12 - Campbell Science CR5000 Data Logger

2.2.7 Dell laptop computer w/PC9000

The CR5000 data acquisition system is operated by a computer coded program. To collect and control necessary data at the live load test, installing the PC9000 computer application and conformed program code on the data acquisition laptop computers was processed. PC9000 is a Windows application for use with the

CR5000. The software PC9000 supports CR5000 program generation, real-time display of data-logger measurements, graphing, and retrieval of data files.

2.2.8 AM16/32 Relay Multiplexers



Figure 13 - AM16/32 Relay Multiplexers

The major function of the AM16/32B Multiplexer is to extend the number of sensors that can be measured by a datalogger. The AM16/32B is connected between the sensors and the datalogger. The AM16/32B is intended for use in applications where the number of required sensors exceeds the number of datalogger input channels. (AM16/32 Campbell Scientific, Inc. 2008) Mechanical relays in the AM16/32B connect each sensor channels in turn to a common output destined for the datalogger. The user program advances the multiplexer through the sensor channels making measurements and storing data.

2.3 LAB TEST

For the lab test, the BDI transducer and the Vishay strain gage were attached on the bottom side of each experimental concrete block which measured 3”W x 3”H x 12”L. Figure 14 shows two concrete blocks prepared for the lab test. In advance, the laptop computer to be used in the live load test, CR5000 and Multiplexer were connected to two sensors. INSTRON 1331 servohydraulic system was used for the 3 point flexure test. The INSTRON 1331 testing machine can maintain constant cross-head speeds ranging from quasi-static (0.08 mm/sec, ASTM Standard D1621) to 250 mm/sec with a closed-loop servo-controlled system.

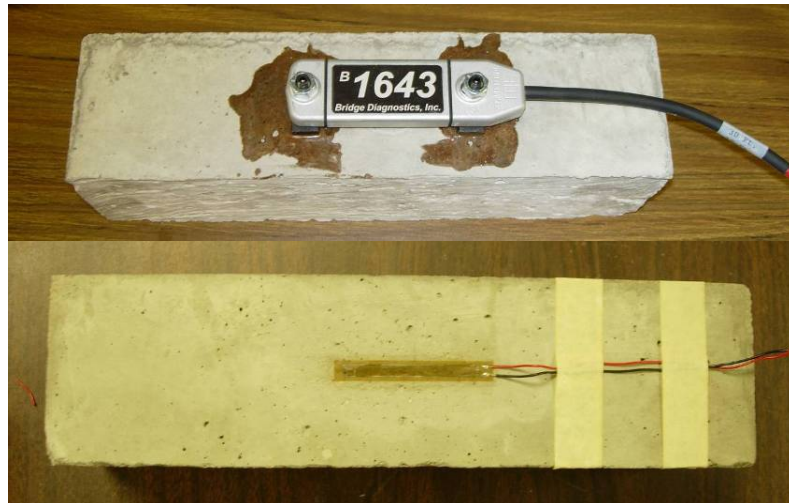


Figure 14 - Sample Testing Concrete Blocks

Since this lab test is mainly focused on connection verification and data calibration between all sensors and data acquisition system, the load rate during the concrete block test was set to an arbitrary rate of 150 lb/min. The Bluehill software used in the test automates data acquisition, machine control, analysis, and reporting for a wide range of test requirements including tension, compression, flexure, friction, peel/tear and simple cyclic. For the test results, a load versus deformation graph was obtained. Test data was recorded in CR5000 simultaneously during the flexure test. Raw data obtained by CR5000 was converted into a readable format according to a pre-programmed formula suggested by BDI. Technical maneuvering of INSTRON was made by the lab technician at the University of Maryland, College Park. Figure 15 and Figure 16 show the set up of the lab test.



Figure 15 - Vishay Strain Gage Flexure Testing



Figure 16 - BDI Strain Transducer Flexure Testing

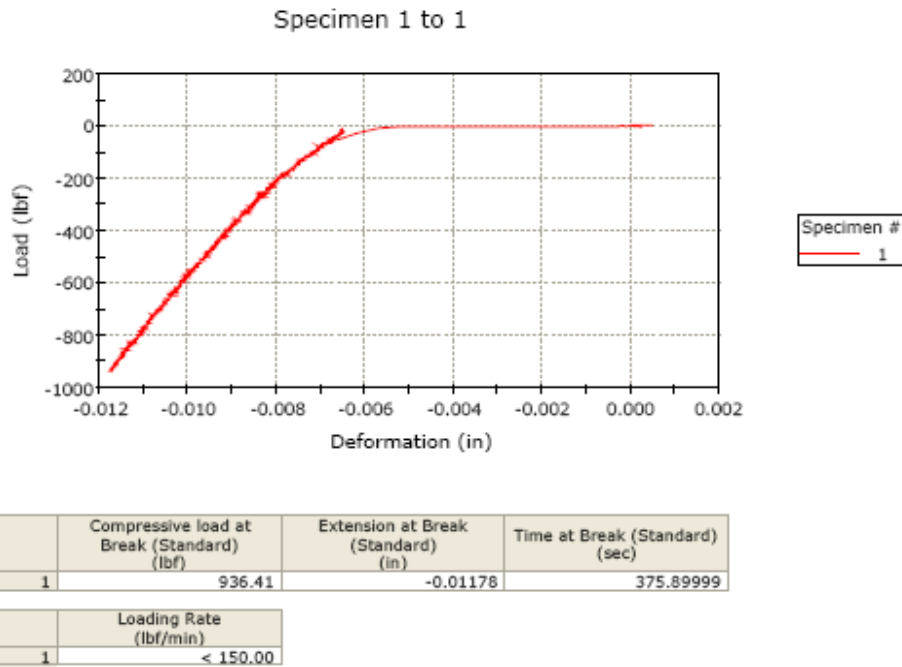


Figure 17 - INSTRON Sample Result

Figure 16 above shows the 3-point flexure test load-deflection sample result generated by Bluehill software. Through the lab test, the operation of all strain sensors and data acquisition systems were checked.

2.4 LIVE LOAD TESTS

2.4.1 Installation and Field Setup

Before the live load tests, sensor installation was completed by the research team on October 14, 2008. Using the lead wires, the connection between four BDI transducers and the data logger was completed on November 20, 2008, the same day as the field test. All sensors were connected to the data logger correctly and the connection was checked by each sensor's specific resistance value using the multi-meter. Access to the underside of testing bridge was enabled by using a float. The Maryland State Highway provided all access, maintenance of traffic and the loaded testing vehicle.

After completion of sensor installation, live load tests were prepared with a two-axle pre-loaded dump truck. Truck paths were decided according to the sensors' locations for obtaining the better strain data. The speed of the truck was crawling, at 5 miles/hour, and 20 miles/hour for each prescribed path. For the live load test, two sets of the transverse post-tension forces were applied to rods A, B, C, and D as Table 2.

Rod	Post-Tensioning Force			
	A	B	C	D
Set 1	30 kips	80 kips	80 kips	80 kips
Set 2	80 kips	80 kips	30 kips	30 kips

Table 2 - Set of Post-Tensioning Force

The post-tensioning force is adjusted for each set before the test truck crossed the bridge. This transverse post-tension rod was adjusted to 80 kip force and 80 kip force after the truck finished crossing the first 3 paths under the 30 kips and 80 kips post-tensioned bridge. Using three different vehicle speeds, each different path (the left wheel of the test truck passed over Beam-2, Beam-4 and Beam-out (furthest apart- load on Beam-8 and Beam-10) were tested and the truck crossing from each path were tested twice to confirm data reproducibility and to establish the reliable characteristics of the deck behavior. When the test truck was crossing over the structure, strain data was recorded simultaneously in the CR5000 Data Logger. Data logger recorded its strain value in every one second. Figure 18 shows three different paths.

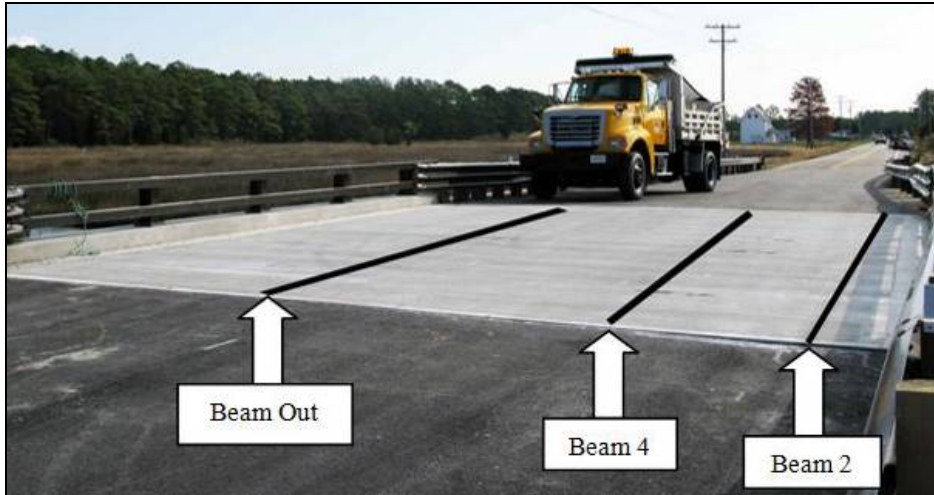


Figure 18 - Paths of Test Truck (Position of Left Wheel of Test Truck)



Figure 19 - Data Acquisition System during Monitoring

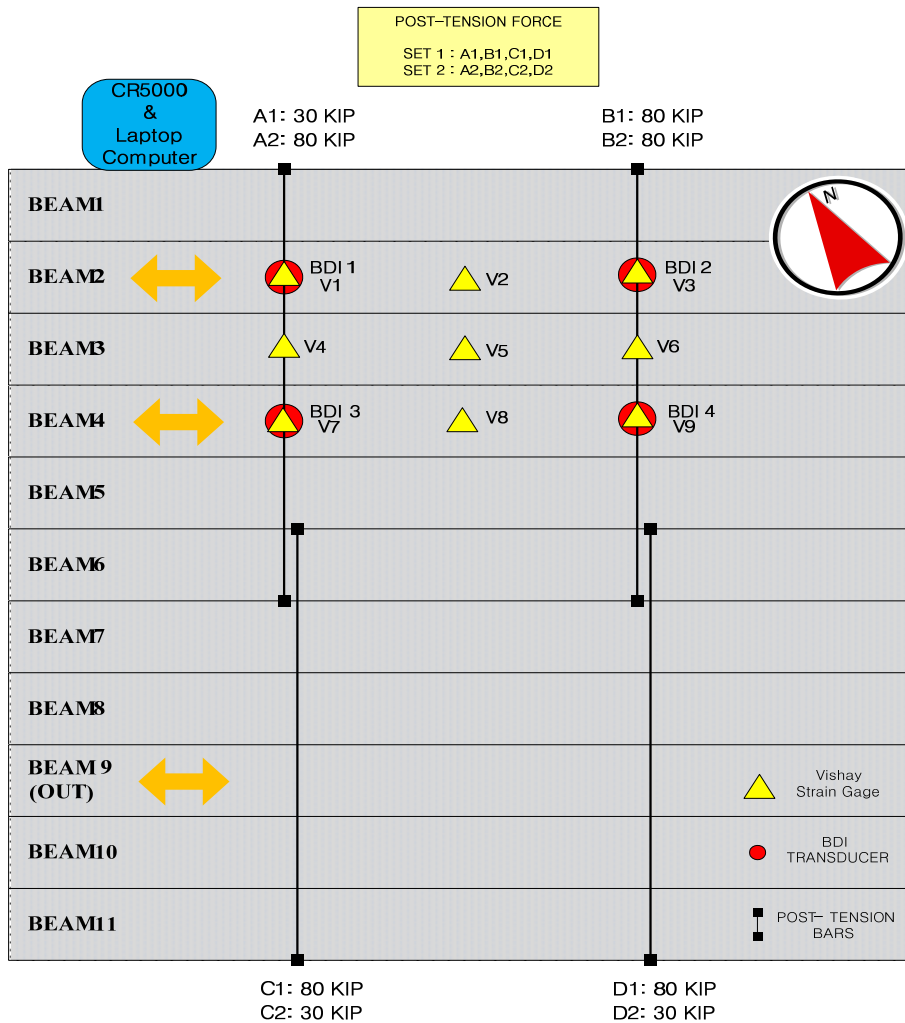


Figure 20 - Summary of Live Load Test Set-Up

2.4.2 Test Vehicle

Weights and dimensions of the actual trucks were recorded before the live-load experiments. Load of the vehicle was weighed at the weighing station. The vehicle and load configurations are summarized in the following figures. Total weight of vehicle is 34,780 lbs. It is a 2-axle truck weighing 5,530 lbs in each front wheel and 11,860 lbs in each rear tandem. The distance between the two front wheels is 6 feet, and the distance between the front and rear wheels is 14 feet. The truck driver was instructed to drive along the designated path marked by masking tape for each passage.



Figure 21 - Testing Vehicle

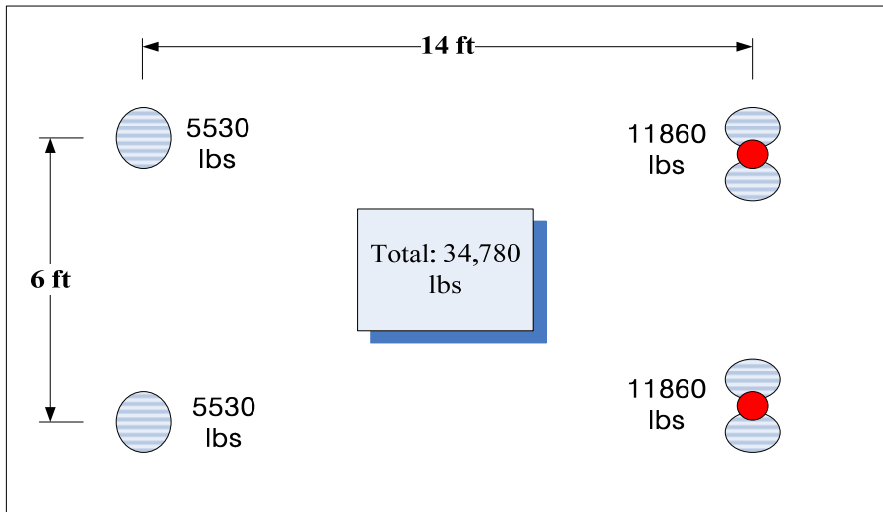


Figure 22 - Vehicle Load Configuration

2.4.3 Result of Live Load Test

The PC9000 program was initialized to retrieve data from CR5000. As the CR5000 collected data from the sensors, the test truck started its path. Data was retrieved in the laptop computer in raw data form. Therefore, the raw data was first converted into the strain format using preprogrammed gage factor calculation, and then plotted as a graph. Table 3 and Table 4 describe crossing of the test truck on Beam-2 at crawl speed. The maximum strain comparison on the same location between BDI transducers and Vishay strain gage is described in each table. As indicated, the first max strain (Max1) location is when the front wheels of the test truck crossed the sensor location. In the same manner, the second max strain (Max2) was when the rear wheels of test truck crossed the sensor location. Corresponding Vishay strain data to the time when BDI maximum data occurred is also described below the BDI strain data.

Truck Left Wheel on Beam 2		BDI 1		BDI 2		BDI 3		BDI 4	
Set1 / Crawling		Max1	Max2	Max1	Max2	Max1	Max2	Max1	Max2
Time	Second	24	29	28	34	24	29	28	34
BDI Strain	(10 ⁶) Inch	7.38	14.99	6.09	10.72	6.48	14.61	3.93	6.75
Corresponding Vishay Strain @ Same Time	Vishay 1	16.32	12.72						
	Vishay 3			28.02	17.07				
	Vishay 7					11.59	30.96		
	Vishay 9							12.91	1.24

Table 3 – Summary of Maximum Strain in Set 1

Truck Left Wheel on Beam 2		BDI 1		BDI 2		BDI 3		BDI 4	
Set2 / Crawling		Max1	Max2	Max1	Max2	Max1	Max2	Max1	Max2
Time	Second	15	24	22	29	15	24	22	29
BDI Strain	(10 ⁶) Inch	6.94	17.03	7.23	12.79	5.95	14.33	3.61	6.64
Corresponding Vishay Strain @ Same Time	Vishay 1	0.23	9.87						
	Vishay 3			12.9	4.49				
	Vishay 7					10.12	2.84		
	Vishay 9							13.67	1.54

Table 4 - Summary of Maximum Strain in Set 2

Maximum strain data of both Vishay strain gage and BDI transducer shows the same trend which is a higher strain under the heavier load (rear wheel) than the front wheel. Moreover, the strain values of BDI sensors under the two different sets of post-tensioning forces illustrates that two sensors aligned in transverse directions produced

the identical strain response: BDI1-BDI3 and BDI2-BDI4. Unlike the BDI transducers, the Vishay strain gage constructed less accurate data. As an example of demonstrating full length in strain data trend, BDI raw data is plotted in Figure 23.

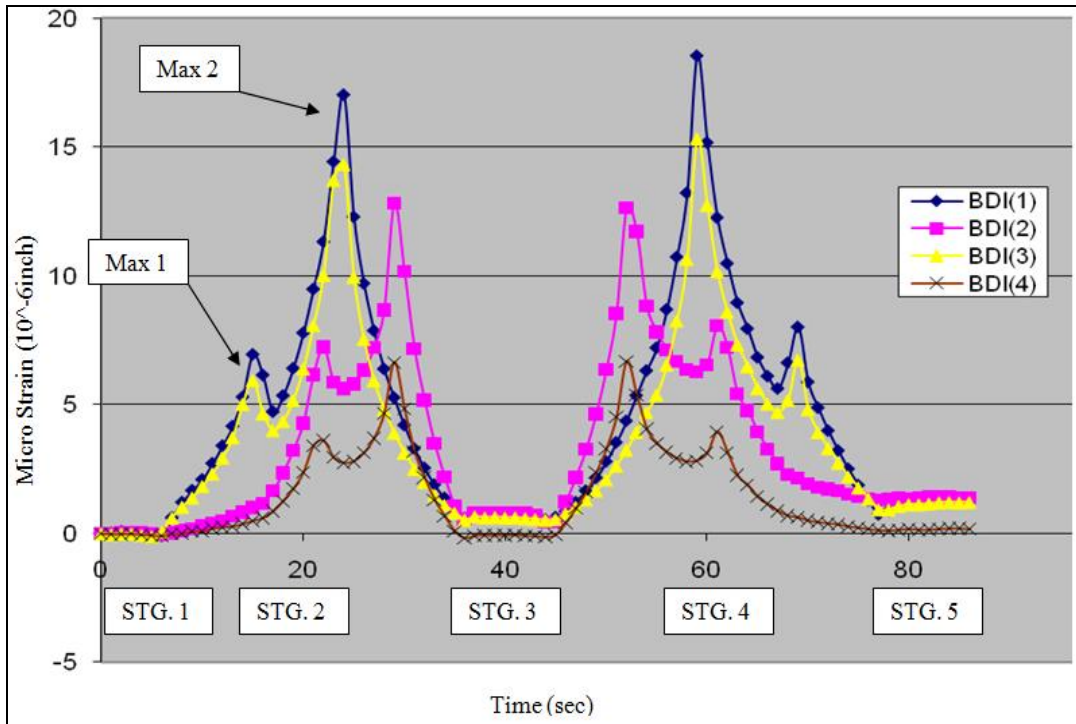


Figure 23 - BDI Gages Scrawling on Beam2

As indicated in the figure above, there are five divided stages in the strain graph. The first and second maximum strain locations are indicated with thick arrows. The first stage shows an almost straight line representing the test truck approaching the bridge. At this stage, the test truck did not have a contact yet on the bridge slab. On the second stage, the test truck made its contact with its front wheel and created changes in the resistance values of the sensors. After the first contact, the crossing of the front and rear wheels over the sensors generated two maximum strain data respectively. Another straight line, the stage 3 in the middle of the graph, stands for the time when the truck is out of contact with the bridge. For this specific graph (Crawling/Beam2/Set1), the test truck was backing. Therefore, the graph in each sensor shows the reflection shape of the first crossing data. In addition, the maximum strain occurs in the same time coupled as BDI1-BDI 3 also BDI2-BDI4 due to its

same location in the longitudinal direction. As the final stage, the test truck is out of contact with the bridge. From this one example of truck-crossing strain data, the reproducibility of strain data is confirmed and reliability of data is acquired. The further live load test detail is added in the appendix.

During the live load test, CR5000 also recorded strain data from Vishay strain gage. Though all sensor resistance was checked before proceeding to truck run, all Vishay strain gages during 20 mile/hour test were found not to be initiated due to unknown reasons. From the plotted data, it was difficult to figure out the trend of the graphs. The fluctuation of data was random. It is quite obvious that noises were created during the live load test. Therefore, BDI sensors were selected alternatively to analyze the bridge.

Because this live load test was focused on the effects of the different post-tensioning forces, synchronizing the initial position of the test truck was disregarded. Regarding the differences in the test truck speeds during the live load tests, the data arrays from all the tests were difficult to show a relationship. Since the temperature changes were minimal because the duration of the test was short, about 2 minutes in each crossing, they were neglected. Also, all strain data graphs were shifted as necessary by setting the initial strains to be zero for each truck crossing.

3. MODELING

In this chapter, the general description of how the finite element model is built is noted, and the calibration of the generated Finite Element Analysis (FEA) model is introduced. Finite element analysis proposes substantial benefits in accurateness over alternative methods of analysis such as grillage analysis or analytical methods in many specific types of structures. (O'Brien 1999, p. 185) For instance, FEA enables membrane forces to be modeled accurately in structures such as arch, box girder, folded plate or shell structures. In addition, FEA modeling allows greater analytical flexibility enabling the model to be manipulated by material characteristics, which can allow further study.

After data of load-deformation response is obtained from FEA bridge model, it is used to compare the FEA bridge model with data from the live load test. In the FEA calibration section, the FEA bridge model will be adjusted according to the results of the live load test data. To understand the bridge behavior, the full scale of the bridge is created. To generate the FEA model, ANSYS V10 is utilized.

3.1 Sections of ANSYS Bridge Model

The ANSYS bridge model consists of 5 sections: Concrete Beam, Shear Key, Deck, Curb, and Transverse Post-Tension Rods. Figure 24 illustrates the shape of each section. All material properties of each section are identical to the properties of the real bridge. Engineering judgment is determined in which parameters should be adjusted so as to obtain the most accurate model. The selection of adjustable parameters is performed by determining what properties have a significant effect on the strain comparison and determining which values cannot be accurately estimated through conventional engineering procedures.

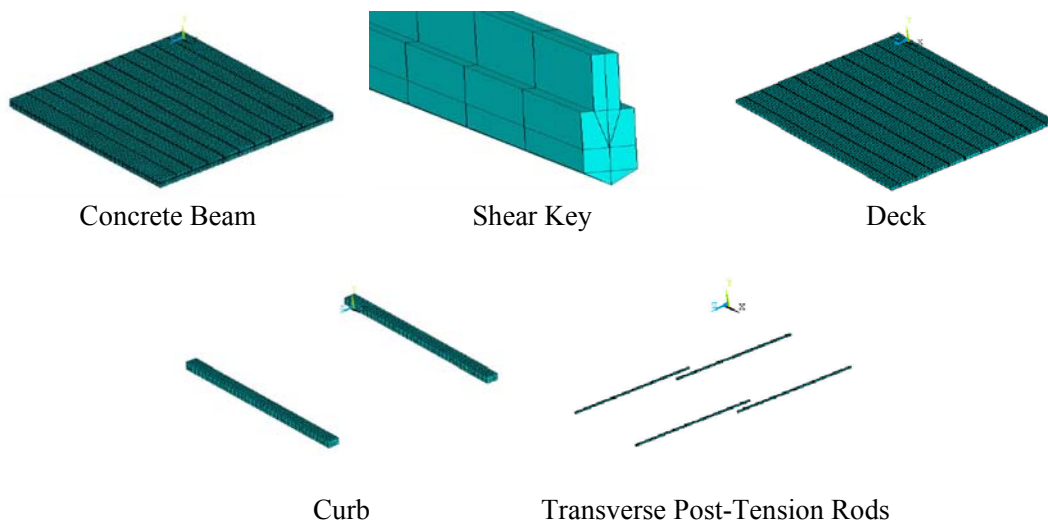


Figure 24 - Types of Sections in FEM Bridge Model

When the shapes of the computed and measured response histories are off, the boundary conditions or the structural geometry are not well represented and must be refined. Figure 25 shows the completed FEA bridge model.

3.2 Material Property

The information of properties in each element is obtained from the general notes in the construction plan. They are in compliance with SHA specifications dated January 2001 and special provisions for materials and construction AASHTO standard specifications for highway bridges dated 2002.

Material	Property
Concrete	-Reinforcing steel design: $f_s = 24,000$ psi -Structural steel design: elastic design method
Cast-In-Place Concrete	-Cast-In-Place curbs on superstructure and cast-in-place curbs at wing walls shall be mix no. 6 (4,500 psi) -Superstructure overlay shall be mix no. 8 (4000 psi) shall be mix no. 3 (3,500 psi)
Prestressed Concrete	-Concrete for prestressed slabs shall have a strength $f'_c = 7,000$ psi and a strength $f'_{ci} = 5,800$ psi at transfer of prestress
Pretensioning Steel Strand	-Pretensioning steel strand s shall consist of 1/2" diameter 7-wire bright low relaxation strands conforming to the requirements of M203 grade 270 -Each 1/2" strand shall be pretensioned to 31,000lb (0.75 f'_s), have an ultimate strength of 41,300 lb and yield strength of 35,000 lb
Reinforcing Steel	-Reinforcing steel shall conform to ASTM A615, grade 60.

Table 5 - Material Property

3.3 Modeling Method

Measuring strain from the live load test can be utilized in understanding the bridge behavior. In addition, it can also become a good developmental tool of the accurate finite element model of the bridge, especially in the calibration process. In performing a comparison of in-field measured data and calculated data by a finite element analysis program, it is essential that the created finite element model represents the identical strain response as the actual bridge behavior. Therefore, creating the same geometry of actual bridge and boundary conditions was required.

In ANSYS modeling, two methods can be used: solid modeling and direct generation. Solid modeling method first selects the geometric boundaries of the model. Then, establishing controls over the size and desired shape of the elements follows. Afterward, ANSYS generates all the nodes and elements automatically. On the other hand, using the direct generation method can give convenience in simple modeling and complete control over geometry and numbering of all nodes, sizes, and connectivity of all elements prior to defining these entities in the ANSYS model. Between the two methods, the method of direct generation is selected. In addition during the modeling process, an FEA model was created using command prompt line input other than the Graphical User Interface (GUI).

3.4 Loading and Boundary Condition

Loads are applied in a manner similar to the actual live load test. A load of the test truck, defined by a two-dimensional group of point loads, is located on the finite element bridge model at discrete locations on the same path that the test truck was driven during the live load test. Locations for obtaining strain data were identical to those in the field so that strains can be computed at the same locations under the same loading conditions.

During model calibration process, two general rules were applied. When the shapes of the computed strains using the finite element model are similar to the measured strain records but the magnitudes are incorrect, this implies that member

stiffness must be adjusted. (Bridge Diagnostics, Inc. 2009) When the shapes of the computed and measured response histories are not very similar, which indicates the boundary conditions or the structural geometry is not well represented, then it must be refined. (Bridge Diagnostics, Inc. 2009) It is recommended to ensure that the finite element model is producing results that can be used for study. And, any model should be calibrated with good experimental data, which will provide the proper modeling parameters needed for later use. (Wolanski 2004, p. 64) In some cases, an accurate model cannot be obtained, particularly when the responses are observed to be non-linear with load position.

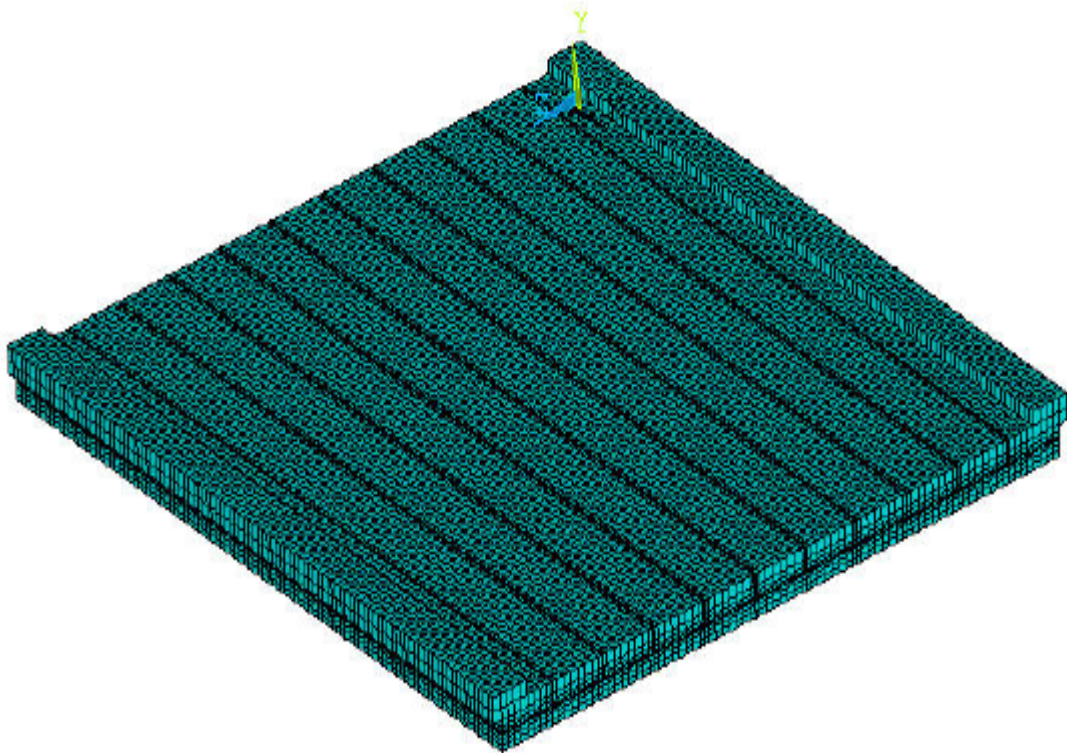


Figure 25 - Isometric View of the Bridge Mode

3.5 Result of Finite Element Analysis

As noted in the previous section, the finite element bridge model was subjected to experiencing the identical loading application in identical locations: Post-Tension Set1 and 2, at the Location of BDI 1, 2, 3, and 4.

Two different paths, Beam2 and Beam4 were selected. The following Tables 6 and Table 7 represent the ANSYS program results with using the completed finite element model. Only the maximum strain data was obtained for easy comparison with measured live load test data.

	Path: Beam2	
Post-Tension Set	Set1: 30-80/80-80	Set2: 80-80/30-30
Location @	Maximum Micro-Strain	Maximum Micro-Strain
BDI1	16.01	16.70
BDI2	15.99	16.06
BDI3	14.07	14.82
BDI4	14.25	14.34

Table 6 - Finite Element Model Result - Beam2

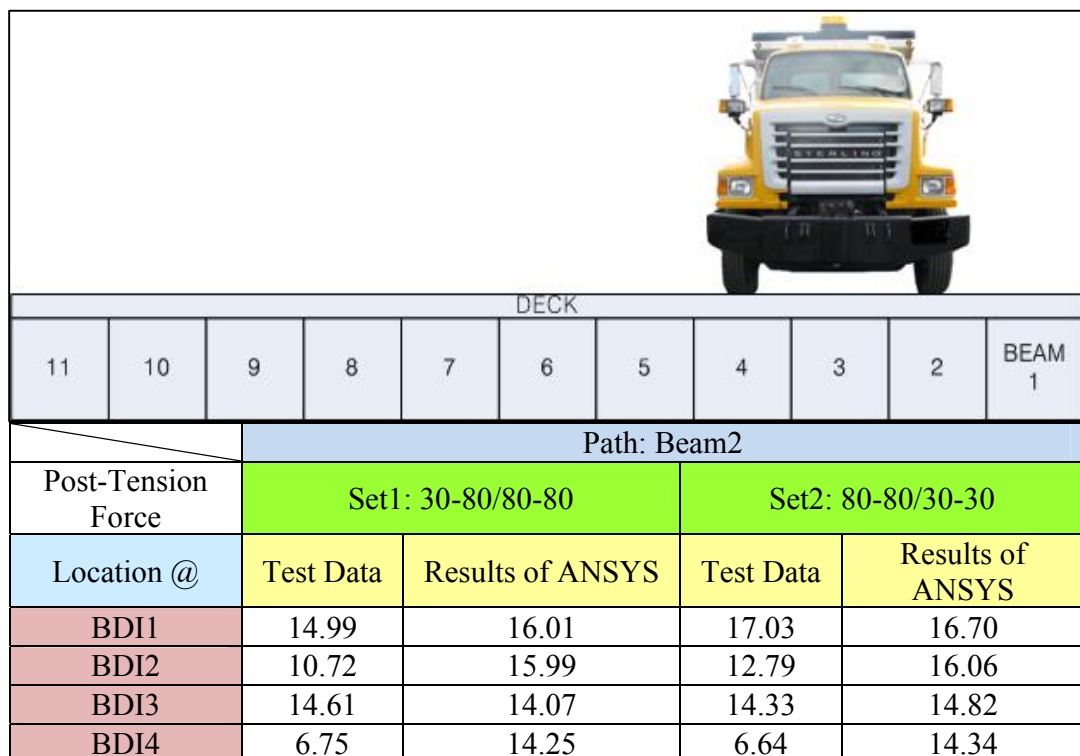
	Path: Beam4	
Post-Tension Set	Set1: 30-80/80-80	Set2: 80-80/30-30
Location @	Maximum Micro-Strain	Maximum Micro-Strain
BDI1	7.01	7.69
BDI2	6.98	7.09
BDI3	13.55	14.29
BDI4	13.84	13.95

Table 7 - Finite Element Model – Beam4

4. SUMMARY OF RESULT

The key purpose of this research project is to provide confidence in using a new design of higher post-tensioning force. During this project, the field test data and FEA model were utilized to understand the bridge behavior under high post-tensioned forces. This chapter details the comparison and analysis of test results between the live load and as built bridge FEA model.

For validation of the FEA model, BDI strain data obtained from the live load test in vehicle paths of Beam2 and Beam4 is used. Since these strain data from two paths are big in magnitude and maximum value in the live load test, they can accommodate easier and more reliable comparisons than comparison with smaller strain data. Figure 26 and Figure 27 describe the summary of strain between the FEA model and the live load test under two different vehicle paths with two post-tensioning force sets.



DECK										
11	10	9	8	7	6	5	4	3	2	BEAM 1
		Path: Beam2								
Post-Tension Force		Set1: 30-80/80-80				Set2: 80-80/30-30				
Location @		Test Data	Results of ANSYS		Test Data	Results of ANSYS				
BDI1		14.99	16.01		17.03	16.70				
BDI2		10.72	15.99		12.79	16.06				
BDI3		14.61	14.07		14.33	14.82				
BDI4		6.75	14.25		6.64	14.34				

Figure 26 - Summary of Test 1


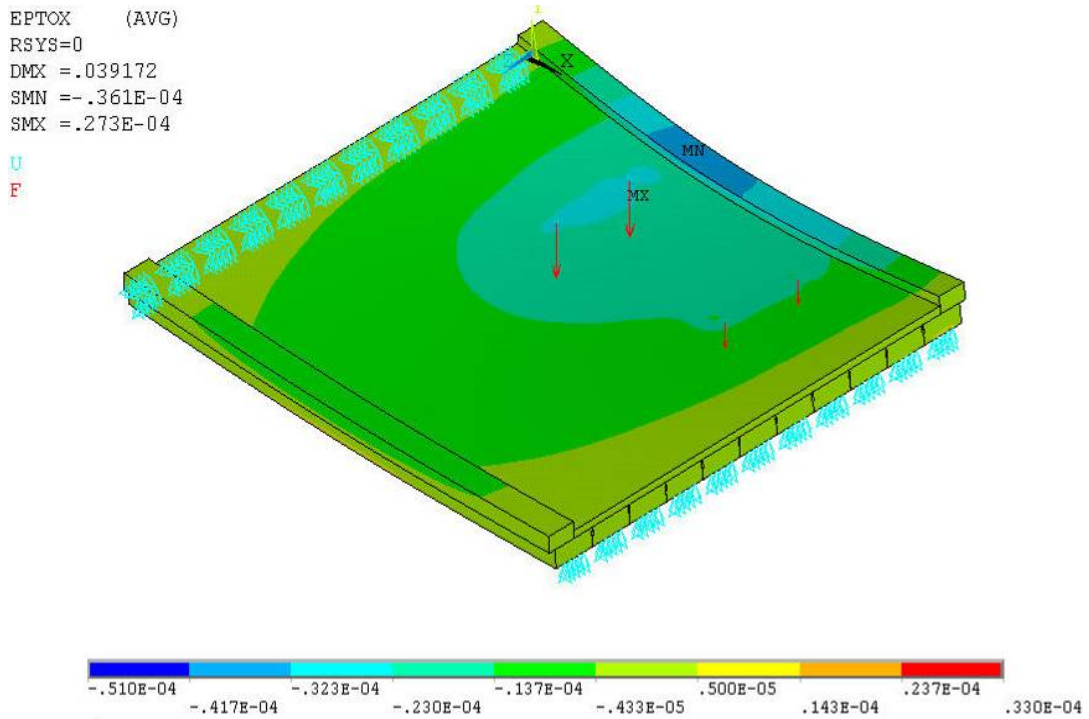
										
DECK										
11	10	9	8	7	6	5	4	3	2	BEAM 1
		Path: Beam4								
Post-Tension Force		Set1: 30-80/80-80				Set2: 80-80/30-30				
Location @		Test Data	Results of ANSYS		Test Data	Results of ANSYS				
BDI1		7.69	7.01		10.00	7.69				
BDI2		4.33	6.98		6.91	7.09				
BDI3		12.41	13.55		15.37	14.29				
BDI4		4.61	13.84		6.82	13.95				

Figure 27 - Summary of Test 2

Test results show the maximum strain data from field live load test and ANSYS model. Observing strain data in BDI1 through BDI3 clearly shows that the maximum field test data is close to the ANSYS model data. As seen on the graph of field test data, the first peak represents the point when the truck's front wheel passed BDI sensors, and the second peak represents the truck's rear wheel passing BDI sensors. The maximum strain of BDI transducer is generated by applying the truck's rear wheel load. Only the first half of the data is used since the second half of the data shows identical results. According to the test data and FEA model, they show the same trend. Therefore, the model can be considered reliable.



Besides the as-built bridge FEA bridge model used in the analysis, simulating the created as-built FEA bridge model or the modified FEA bridge model under the various conditions was also conducted because it can also provide very supportive clues to explain the behavior of the bridge. Therefore, the parametric study was added as a supportive tool in the next chapter.

5. PARAMETRIC STUDY

5.1 Investigation of Model

From the test using the completed FEA model of the as-built bridge, the maximum strain data was obtained. By illustrating the whole picture of strain distribution, behavior of the concrete beams can be explained more clearly. Figure 29 shows the stress distribution of test bridge under three different post-tensioning force. According to the stress distribution in Figure 29, the area of green region is decreasing along higher post-tensioning force: The red color indicates higher strain.

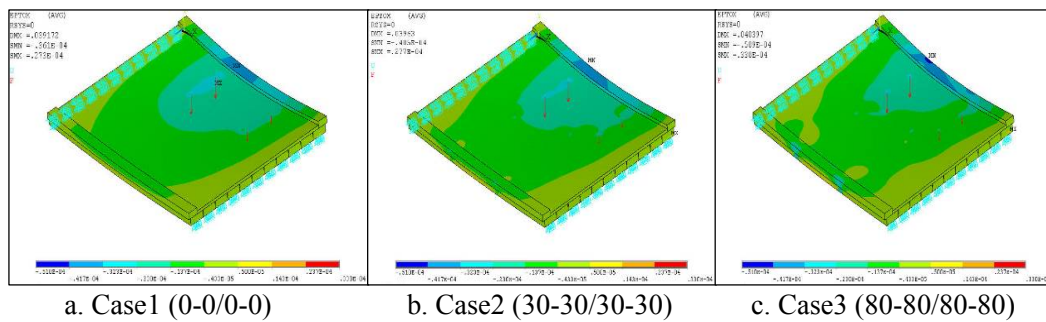


Figure 29 - Longitudinal Strain Distribution of Bridge Model

As the post-tension effect on the concrete beams is understood to be more significantly involved in bridge behavior depending on existence of crack in the shear key, the cracked as well as uncracked ANSYS models were developed in analysis. The resulting analysis was compared with the maximum strain data between the field test and ANSYS models in locations of BDI1 and BDI3. Table 8 and Table 9 summarizes the result of the ANSYS model under three different post-tensioning force using the cracked shear key model and uncracked shear key model. The difference between Case1(zero post-tensioning force) and Case2(30 kips post-tensioning force), Case3(80 kips post-tensioning force) is all less than 3% which is insignificant. In addition, the comparison in analysis for uncracked model presents an increasing trend in strain data coupled with the increase of post-tensioning force. This slight increase can be interpreted as a Poission's effect. Therefore, as the

concrete beam is under compression from the transverse direction, it inclines to expand in the vertical direction.

Boundary: XY, Y	Path – Beam2				
Uncracked	Case1 (0-0/0-0)	Case2 (30-30/30-30)	Case3 (80-80/80-80)	Case1 vs. Case2	Case1 vs. Case3
BDI1	27.253	27.548	28.040	1.08%	2.89%
BDI3	23.624	23.881	24.308	1.09%	2.90%

Table 8 - Uncracked Case of Shear Key

Boundary: XY, Y	Path – Beam2				
Cracked	Case1 (0-0/0-0)	Case2 (30-30/30-30)	Case3 (80-80/80-80)	Case1 vs. Case2	Case1 vs. Case3
BDI1	28.356	27.614	27.904	-2.62%	-1.59%
BDI3	25.166	24.091	24.025	-4.27%	-4.53%

Table 9 - Cracked Case of Shear Key

In Table 9, the cracked model shows acceptable trend of decreasing strain due to post-tensioning force. However, during the simulation with 80 kips post-tensioning force model, the concrete beam element is found to penetrate each other below the location of shear keys. Figure 30 illustrates the penetration between two concrete beams. The overlapped section in Figure 31 is also showing the beam penetration. Because the penetration between the concrete beams is nonexistent, the current cracked FEA model should be modified.

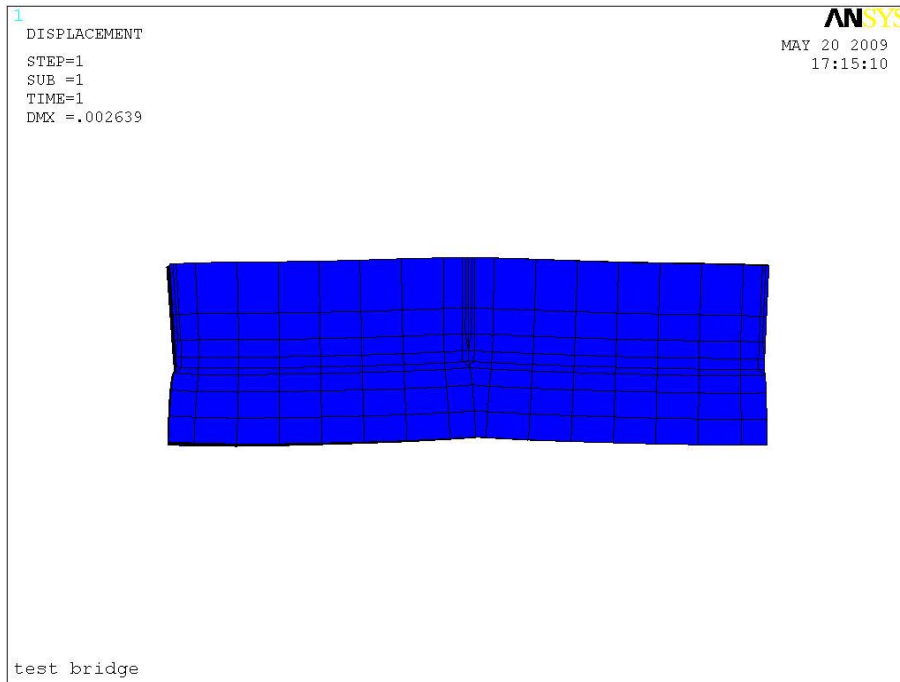


Figure 30 - Concrete Beam Penetration-1

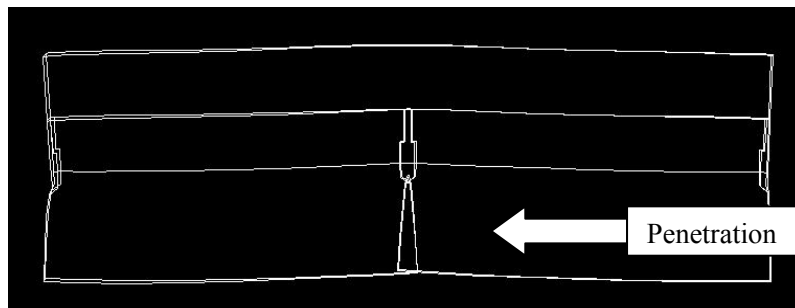


Figure 31 - Concrete Beam Penetration-2

Therefore, the analysis of the first cracked model became irrelevant and not considered in analysis. To avoid overlapping or penetration of elements, the contact element(CONTA174) and target element(TARGE170) were employed to modify FEA model. These two elements were used between the concrete beams. CONTA 174 is brought into play to represent contact and sliding between 3-D target surfaces and deformable surface. TARGE170 is discretized by a set of target segment elements and is paired with its associated contact surface via a shared real constant set. The contact elements themselves overlay the solid elements describing the boundary of a deformable body and are potentially in contact with the target surface, defined by

element TARGE170. With these two elements, impose any translational or rotational displacement, temperature, voltage, and magnetic potential on the target segment element is achievable as well as imposing forces and moments on target elements. (ANSYS users' manual, 1992) Figure 32 and Figure 33 show the geometry of CONTA174 and TARGE170 respectively. And, Figure 34 shows created contact element.

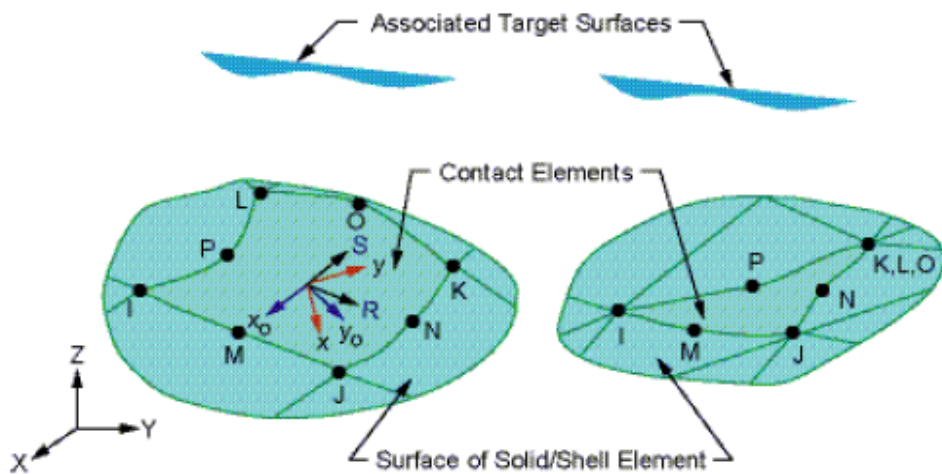


Figure 32 - CONTA174 Geometry

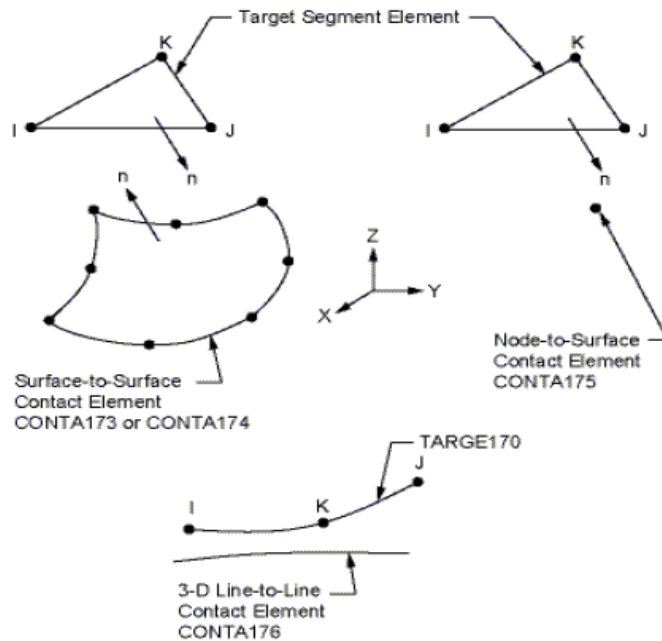


Figure 33 - TARGE170 Geometry

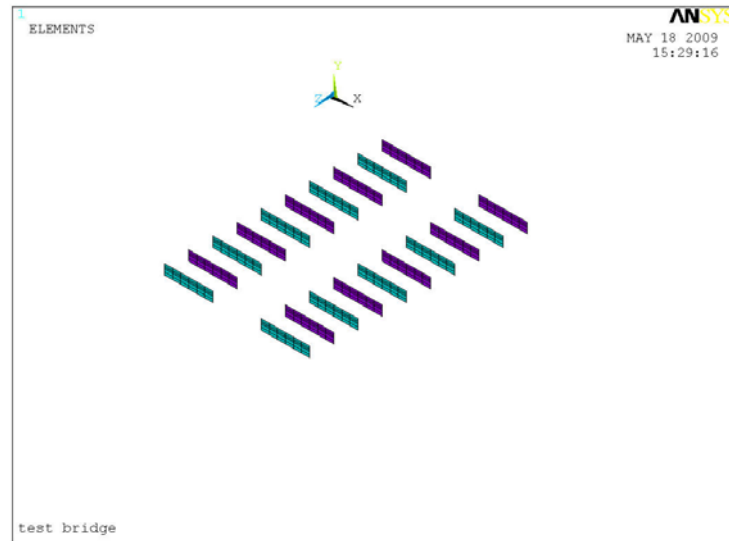


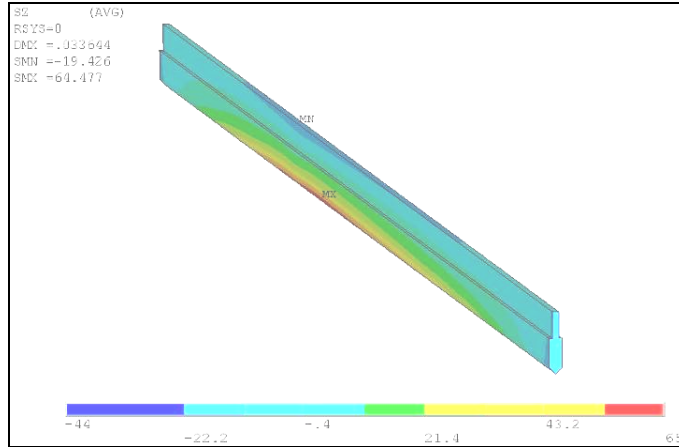
Figure 34 - Contact Element

With modified cracked model, the FEA is performed. Based on the test with new cracked model, it didn't show much difference comparing to uncracked model. Therefore, the direction of FEA simulation with the cracked model shifts to figuring out the specific level of the post-tensioning force that can stabilize strain of concrete beam. Next chapter will present the stabilization graphs by using discretized post-tensioning forces.

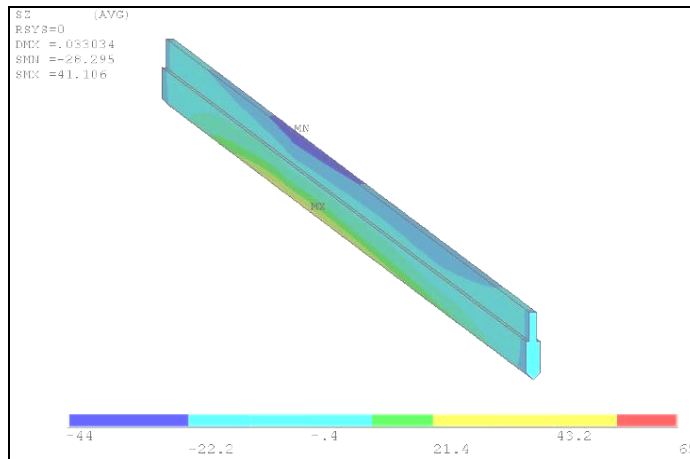
5.2 Shear Key Investigation

First, for the cracked case of shear key, it is challenging to simulate actual structural behavior. We simulated connection between beams as only one point for the cracked model. So, the model can transfer shear force, but, actually, the cracked shear key cannot transfer total shear force. However, we can get the trend from this model which can give us a reference to recognize actual cracked behavior. Referring to the Table 9, it demonstrated that the longitudinal strains decreased under transverse post-tensioning force. That means the transverse bars can increase the integrity of the adjacent precast beams when the shear key is cracked.

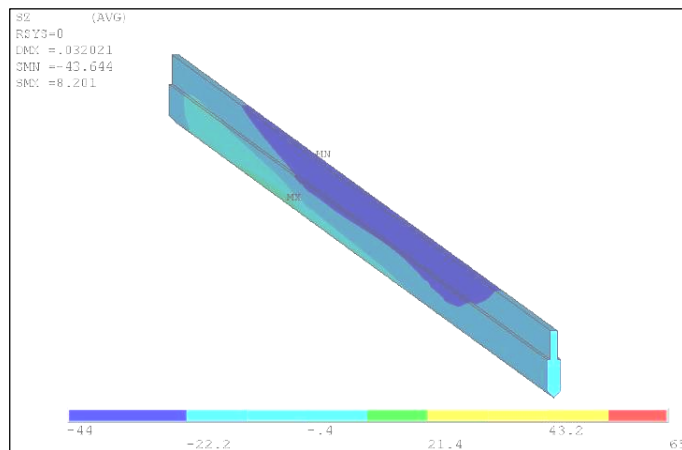
The reason why much higher post-tensioning force does not contribute to reducing the strain is explained via limit load transfer capability of uncracked shear key. Under uncracked shear key environment, the concrete beam does not gain significant benefits from an increment of post-tension force. (Badwan 2007, p. 373) If the shear key cracked, the connection between beams would be weakened, which is not favorable for the structural performance. The role of transverse bars is to help the shear key to stay under compression. Therefore, the transverse compressive stress of the shear key would increase as post-tensioning force increases, which means that it would provide larger safety reserves to prevent shear key cracking. Most proposed shear key design changes are in the direction of increasing the depth of the shear key or increasing the level of transverse post-tensioning. (Huckelbridge Jr 1995, p. 284) (Lall 1998, p. 74-75) Based on the several recent studies have been published, the shear key connection can be significantly strengthened and cracking can be reduced or eliminated by providing adequate transverse post-tensioning (Miller et al., 1999). Figures 35 shows that the transverse compressive stress increased as the forces of transverse bars increased in order of a-b-c.



a. Case1 (0-0/0-0)



b. Case2 (30-30/30-30)



c. Case3 (80-80/80-80)

Figure 35 - Transverse Stress Distribution Diagram of Shear Key

5.3 Sequence of Construction of Shear Key

As described in section 5.2, the shear key has gained strength from the transverse post-tensioning force. Therefore, the current sequence of construction of shear key needed to be ensured whether the sequence of construction allies to the way that can give a benefit to shear key. The Figure 36 and Figure 37 were obtained from the structural standard manual of MDSHA. According to the plan detail, the current Maryland shear key construction standard is set to post-tensioning rod to be tensioned to 30,000 lbs. prior to filling shear keys and placing overlay, which does not contribute shear key strengthening. As stated earlier section, by modifying the sequence of construction of shear key, the bridge can experience less deflection on beams through helping beams to behave monolithically. Therefore, post-tensioning is recommended after the shear key is fully integrated with bridge slab.

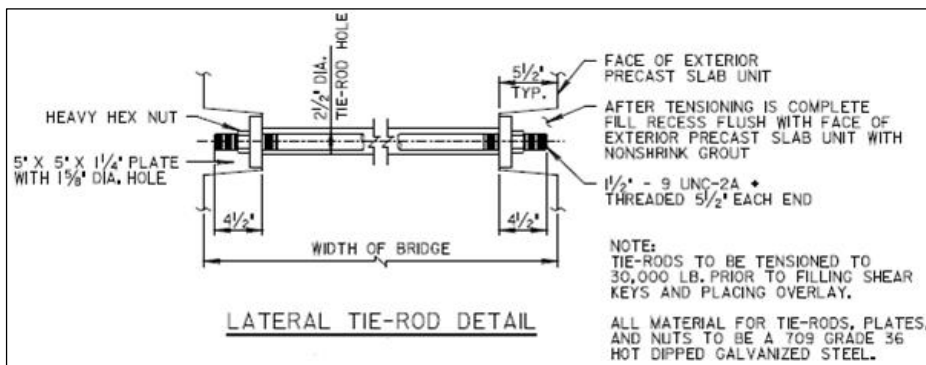


Figure 36 – Lateral Post-Tensioning Rod Detail

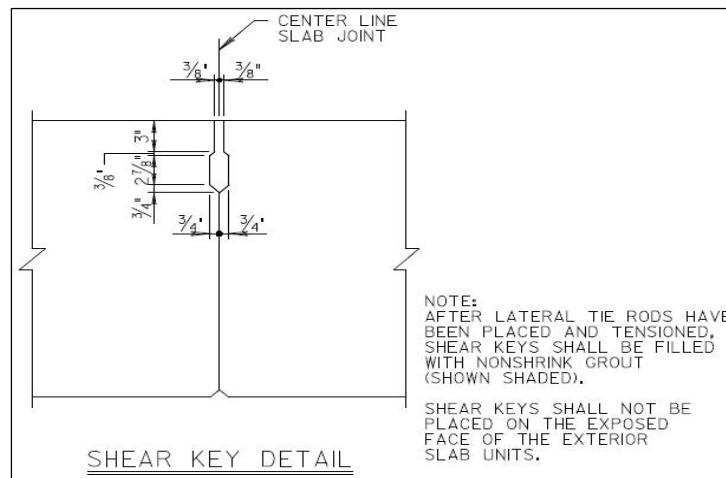


Figure 37 – Shear Key Detail

5.4 Parametric Study on Varying Post-tensioning Forces of the Tested 35'-span Bridge

Table 10 is the current Maryland code of practice - ‘Simple Span Slabs Standard Design Information’ used in designing test bridges. In Figure 38, with zero post-tensioning force, FEA bridge beam behaves independently. Therefore, only Beams with applied load show strain and displacement: the initial strain and displacement in other beams experience zero displacement and strain. As the post-tensioning force increases, strain and displacement significantly decrease and are stabilized approximately at 40 kips. Beams initially loaded share their loads with other beams which were not loaded initially. Displacement and microstrain from all beams get close as post-tensioning force increases.

DESIGN INFORMATION							
SPAN LENGTH (FT)	WIDTH OF BEAM (FT)	DEPTH OF BEAM (FT)	# OF 1/2 IN. DIA. STRANDS	E (IN)	BEAM DL (K/FT)	SIDL (K/FT)	LL (K/FT)
20	4.00	1.25	9	3.75	0.75	0.36	HS27
25	4.00	1.25	12	3.75	0.75	0.36	HS27
30	4.00	1.50	14	4.68	0.90	0.36	HS27
35	4.00	1.50	18	4.58	0.90	0.36	HS25
40	4.00	1.75	20	5.15	1.05	0.36	HS25
45	4.00	2.00	22	6.07	1.20	0.36	HS25
50	4.00	2.25	24	7.08	1.35	0.36	HS25
55	4.00	2.25	32	6.63	1.35	0.36	HS25

Table 10 - Current Maryland Code of Practice Structural Standards Manual MDSHA 2006

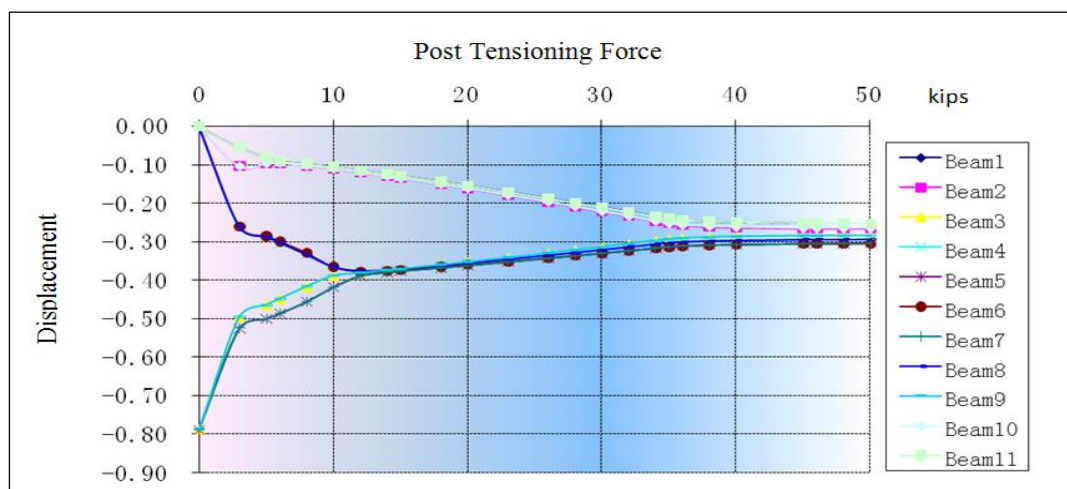


Figure 38 - Displacement of Middle Span

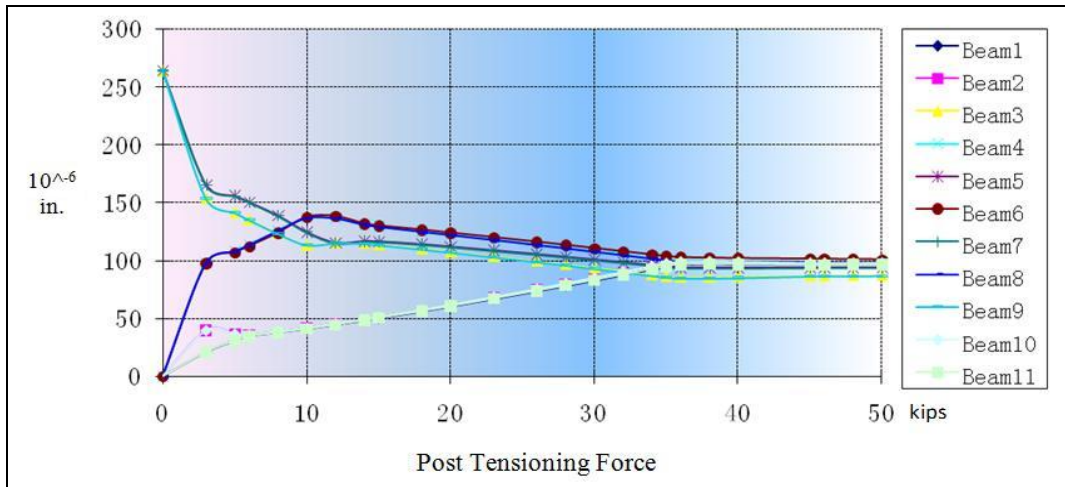


Figure 39 - Microstrain under Post-Tension

Figure 39 above indicates that with the current Maryland code of practice, specifically 30 kips for the test bridge, the strain is not yet stabilized up to 35 kips post-tensioning force. The post-tensioning force is not sufficient to relieve displacement of the bridge. Therefore, the increasing post-tensioning force is recommended to alleviate the displacement of each beam and help the entire structure to endure design vehicle (HS25) more efficiently.

5.5 Parametric Study on Bridges of Other Span Lengths

As an extensive part of section 5.3, this section will give a set of post-tensioning force required to stabilize the beam’s deflection in bridges with other span lengths. As seen in section 5.3, the beam deflection under post-tensioning force of 35 kips is stabilized. Based on the existing design information in Table 10, the analogous analysis as section 5.3 are performed to establish the approximate stabilizing post-tensioning force for the beam deflection. According to the ‘Study of the Impact of the Transverse Post-tensioning Force Required to Make Precast Concrete Slabs as a Single Unit’ by BEST center in 2006, the Table 11 included under the appendix shows several other states’ practices of the transverse post-tensioning force standards. It describes Maryland is using relatively low post-tensioning force in designing comparable class of bridge that has the span length of 35’. For example, the state of New York is using 80 kips of post-tensioning force in

design regardless it is shorter or longer than 50' bridge span. In addition, Massachusetts and Miami is using 44 kips and 82.5/104.5 kips post-tensioning force respectively, which is more than 30 kips that of Maryland's.

STATE	SPAN	BEAM		SHEAR KEY	PT TYPE	LATERAL SPACING	AT DEPTH	PT FORCE	NO. OF TENDONS		GROUT	REMARKS	DATE
		TYPE	DEPTH						WIDTH	LENGTH			
MD	55'	SOLID	27"	48"	7"	1.5" tie rods	18'-4"	15" from bottom	30 kips	2	1 NON SHRINK		2003
MD	50'	SOLID	27"	48"	7"	1.5" tie rods	16'-8"	15" from bottom	30 kips	2	1 NON SHRINK		2003
MD	45'	SOLID	24"	48"	7"	1.5" tie rods	15'	15" from bottom	30 kips	2	1 NON SHRINK		2003
MD	40'	SOLID	21"	48"	7"	1.5" tie rods	13'-4"	13" from bottom	30 kips	2	1 NON SHRINK		2003
MD	35'	SOLID	18"	48"	7"	1.5" tie rods	11'-8"	11" from bottom	30 kips	2	1 NON SHRINK		2003
MD	30'	SOLID	18"	48"	7"	1.5" tie rods	10'	11" from bottom	30 kips	2	1 NON SHRINK		2003
MD	25'	SOLID	15"	48"	7"	1.5" tie rods	8'-4"	9" from bottom	30 kips	2	1 NON SHRINK		2003
MD	20'	SOLID	15"	48"	7"	1.5" tie rods	8'-8"	9" from bottom	30 kips	2	1 NON SHRINK		2003
NY	>50'	HOLLOW	12'-54"	36'/48"	FULL	1.3mm Polystrand tendons	SPAN/2	middle	84.25kips	5	1 NON SHRINK	diaphragm typ. 30mm	1/26/2005
NY	>50'	HOLLOW	12'-54"	36'/48"	FULL	three per hole	SPAN/4	third	84.25kips	5	1 NON SHRINK		1/26/2005
AL	24'	A-TYPE	1'-5"	2'-6"/3'-6"	5"	tie rods	8'	10" from bottom	--	3	1	diaphragm triangle	8/27/2002
AL	34'	A-TYPE	1'-9"	3'-3"/3'-6"	5"	tie rods	13'		--	3	1		8/27/2002
WA		SOLID	12"	48"	FULL	--	--	--	--	--	--		12/2/2005
WA		HOLLOW	18"	48"	FULL	--	--	--	--	--	class 4000D conc.		12/2/2005
WA		HOLLOW	26"	48"	FULL	--	--	--	--	--			12/2/2005
CA	S136	SOLID	12"	36"	FULL	--	--	--	--	--			10/14/1997
CA	S1136	HOLLOW	15"	36"	FULL	--	--	--	--	--			10/14/1997
CA	S1136	HOLLOW	18"	36"	FULL	--	--	--	--	--			10/14/1997
CA	S1V36	HOLLOW	21"	36"	FULL	--	--	--	--	--			10/14/1997
CA	S148	SOLID	12"	48"	FULL	--	--	--	--	--			10/14/1997
CA	S148	HOLLOW	15"	48"	FULL	--	--	--	--	--			10/14/1997
CA	S1148	HOLLOW	18"	48"	FULL	--	--	--	--	--			10/14/1997
CA	S1V48	HOLLOW	21"	48"	FULL	--	--	--	--	--			10/14/1997
OR		HOLLOW	15"	48"	7"	TIE RODS	4'	mid-depth	39.25Kips	--	1 non-shrnk with bck rod	DIAPHRAGM	2002
OR		HOLLOW	18"	48"	7"	TIE RODS	4'	mid-depth	39.25Kips	--	1 non-shrnk with bck rod	6'-12"	2002
OR		HOLLOW	21"	48"	7"	TIE RODS	4'	mid-depth	39.25Kips	--	1 non-shrnk with bck rod		2002
OR		HOLLOW	26"	48"	7"	TIE RODS	4'	mid-depth	39.25Kips	--	1 non-shrnk with bck rod		2002
OR		HOLLOW	30"	48"	7"	TIE RODS	4'	mid-depth	39.25Kips	--	1 non-shrnk with bck rod		2002
VA	>20'	circular voids			7"	tie rods	--	--	39kips	--	--		2001
VA	>20'	circular voids			7"	tie rods	--	--	31.6kips	--	--		2001
MA	>55'	solid/void	12'/15'-48"	36'/48"	full	0.6" dia seven strands	ends, midspan	mid depth	44kips	3	1	diaphragm typ.	05/2005
MA	>55'	solid/void	12'/15'-48"	36'/48"	full	0.6" dia seven strands	ends, quatr points	mid depth	44kips	5	1	12" wide	
MI	>50'	voided	12'-42"		full depth	--	--	--	82.5/104.5kips	3	--		2003
MI	50'-62'	voided	12'-42"		full depth	--	--	--	82.5/104.5kips	3	--	diaphragm = 8"	2003
MI	62'-100'	voided	12'-42"		full depth	--	--	--	82.5/104.5kips	4	--		2003
MI	>100'	voided	12'-42"		full depth	--	--	--	82.5/104.5kips	6	--		2003
SC	30,40,50	circular void	1'-9"	3'-0"	7"	7 - wire low relaxation	middle third	10.5' from bottom	31 kips	2	1	diphragm = 8" wide	12/21/2005
SC	60'	circular void	2'-0"	3'-0"	7"	grade 270 strands	middle third	12" from bottom	31 kips	2	1	diphragm = 8" wide	12/21/2005

Table 11 - Other States' Practices of the Transverse Post-tensioning

For observing the deflection stabilizing point in various bridge span lengths, each finite element bridge model with different span lengths is developed and analyzed. Figure 40 and shows typical bridge cross section for 35', 40', 45', 50', and 55' Span. In addition, Figure 41 is typical finite element model. The finite element model analysis results for each different bridge span lengths are demonstrated through Though Figure 42 to Figure 46. Each table provided the stabilizing post-tensioning forces and they are tabulated in Table 12.

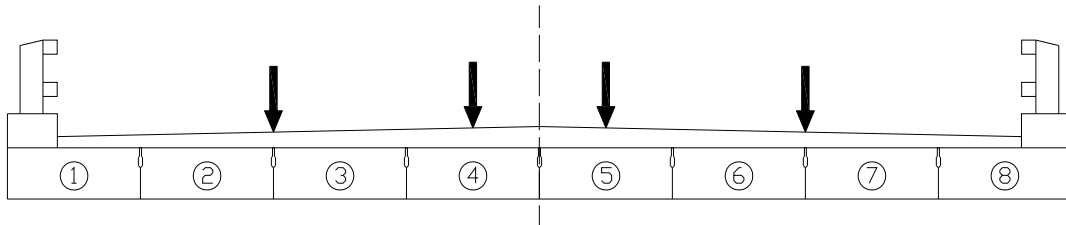


Figure 40 – Cross Section of Analyzing Bridge (35', 40', 45', 50', and 55' Span)

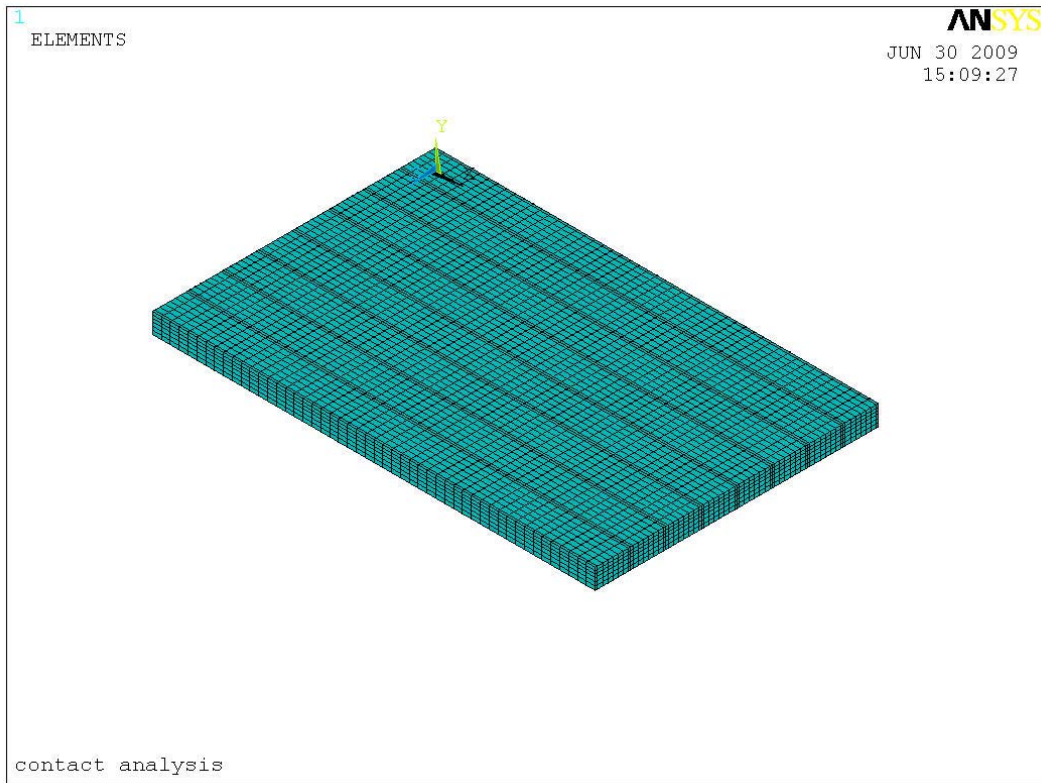


Figure 41 – Finite Element Model of Bridge as Maryland Code of Practice

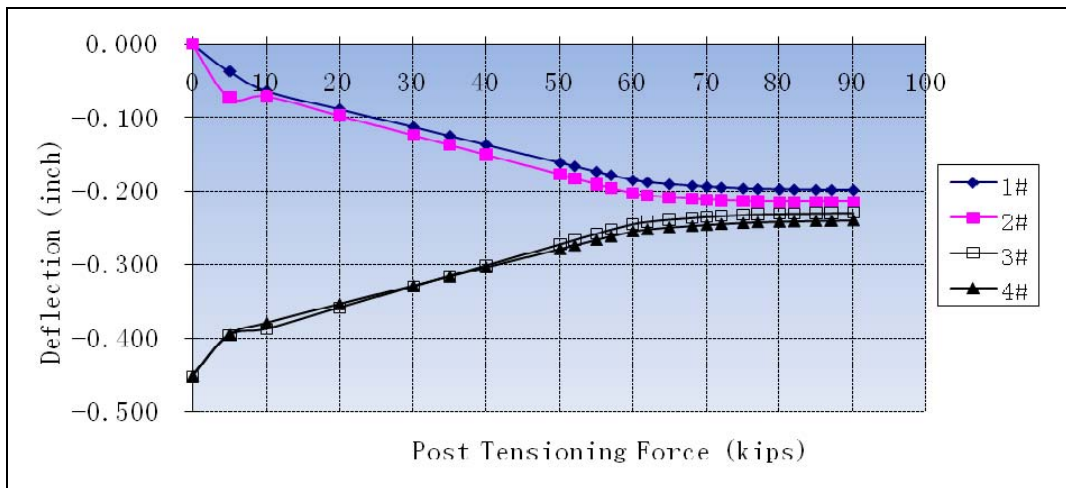


Figure 42 – Stabilization of Deflection on 35ft Span Bridge

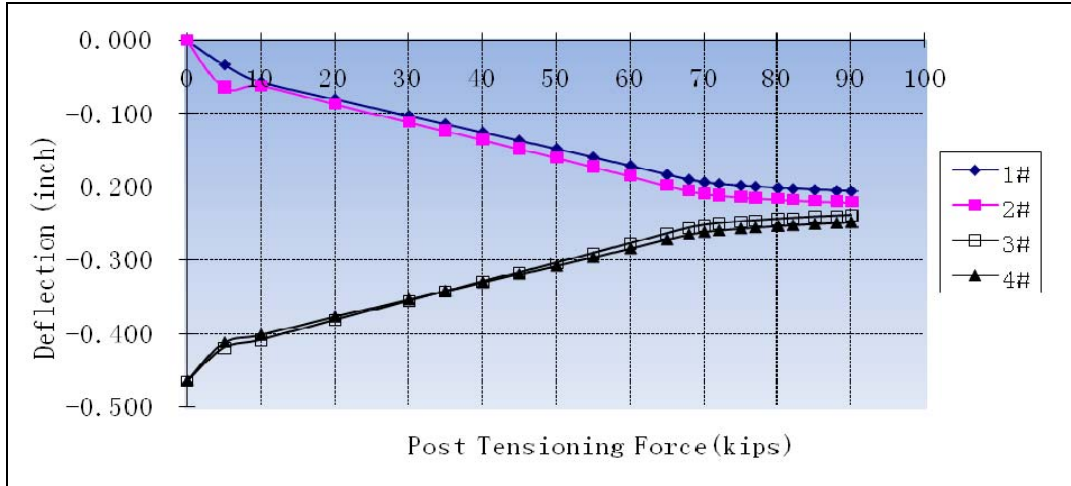


Figure 43 - Stabilization of Deflection on 40ft Span Bridge

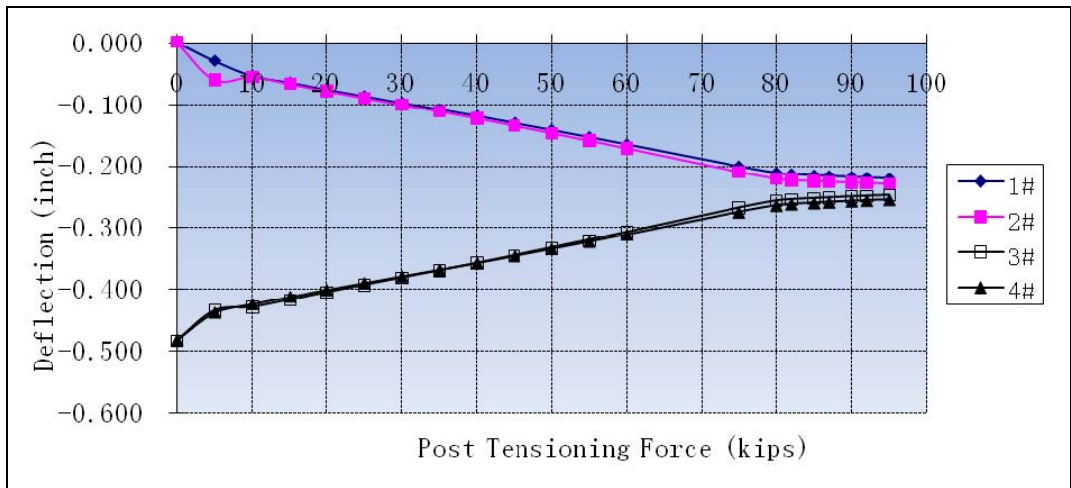


Figure 44 - Stabilization of Deflection on 45ft Span Bridge

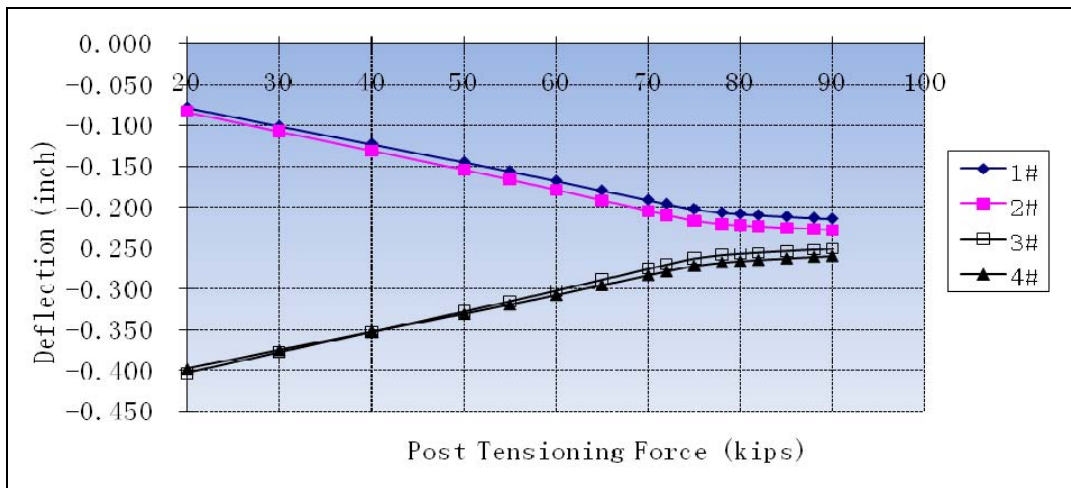


Figure 45 - Stabilization of Deflection on 50ft Span Bridge

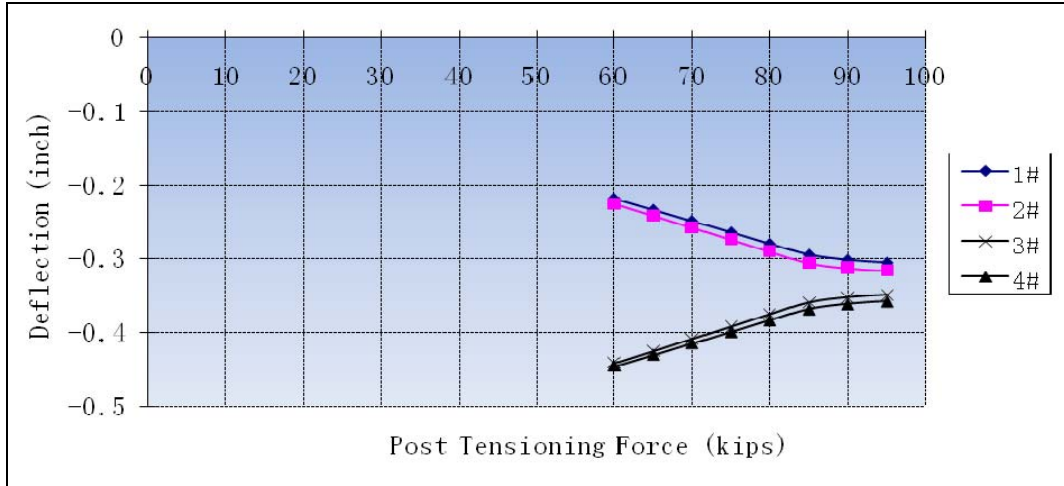


Figure 46 - Stabilization of Deflection on 55ft Span Bridge

Span Length	Approximate Stabilizing Transverse Post-Tensioning Force
35'	60 kips
40'	70 kips
45'	80 kips
50'	80 kips
55'	90 kips

Table 12 - Transverse Post-Tension Required in Stabilizing Deflection of Beams

The points 1, 2, 3 and 4 in Figure 42 to Figure 46 indicate the measuring displacement locations respectively. According to the Table 12, the trend of stabilizing points of transverse post-tensioning force along different bridge spans illustrates that higher transverse post-tensioning force required for having a stable deflection as along longer bridge span length.

6. CONCLUSION

In this research, the comparison between the FEA model and the live load test data showed that a tightly integrated modular slab bridge system with higher post-tensioning forces can provide better structural integrity. From the refined ANSYS model, strain results were very close to those from the field test data. Furthermore, the comparison between the field test data and measured data from the FEA model also has drawn the conclusion that the effect of transverse bars before cracking of the shear key was insignificant.

The analysis of the FEA model under different post-tensioning forces proved that the post-tensioning rods under the uncracked shear key condition are not taking into a significant action. However, once the shear key is cracked, the post-tensioning rod is brought into an eminent role in preventing the structure from undergoing further deterioration. In addition, it eventually will help a structure to be reinforced so that it behaves in monolithic manner.

In FEA model testing with an HS25 truck, which is different from the test truck but the same design truck for the bridge, the current code of practice in Maryland is recommended to be modified in its sequence of construction of shear key and increase its post-tensioning force to a higher level so that the shear key is strengthened by the post-tensioning force producing less cracking issues on the shear key section. This will give the bridge a better service life and more structural integrity in the future. In depth future research and monitoring will help to gain more confidence using a new level of post-tensioning forces.

REFERENCES

- “Study of the Impact of the Transverse Post-tensioning Force Required to Make Precast Concrete Slabs as a Single Unit”, Report to SHA by Bridge Engineering Software and Technology (BEST) Center, Revision 5, University of Maryland, College Park, 2006
- Construction Plan, State of Maryland Department of Transportation State Highway Administration Office of Bridge Design Prestressed Concrete Slab Panel Br. N0. 0901100
- Structure Number 0901100, Maryland State Highway Administration Database.
- Vishay. 2008 General Purpose Strain Gages - Linear Pattern 20CBW: Malvern, PA. (PDF version of document downloaded April 30, 2009)
- "Strain gauge." *Wikipedia, The Free Encyclopedia*. 1 Nov 2009, 03:09 UTC. 10 Nov 2009
<http://en.wikipedia.org/w/index.php?title=Strain_gauge&oldid=323215576>.
- "Strain Transducer for Structural Testing." *Bridge load testing & rating, structural monitoring*. Bridge Diagnostics, Inc. Web. 10 Nov. 2009.
<http://bridgetest.com/products/strain_transducers.html>.
- Campbell Scientific, Inc. 2006 CR5000 Measurement and Control System Operator's Manual: Logan, Utah. (PDF version of document downloaded April 30, 2009)
- Campbell Scientific, Inc. 2008 AM16/32 Relay Multiplexer Instruction Manual – CR5000 Measurement and Control System: Logan, Utah. (PDF version of document downloaded May 4, 2009)
- O'Brien, Eugene J., and Damien L. Keogh. *Bridge Deck Analysis*. London: E & FN Spon, 1999: 185.
- "Load Test and Rating Report Steel Truss Bridge”, Bonham Butler County, Ohio, *Bridge load testing & rating, structural monitoring*. Bridge Diagnostics, Inc. Web. 12 Nov. 2009. <<http://www.bridgetest.com/support/docs/Bohnam.pdf>>
- ANSYS users' manual for revision 10.0, Part I. Elementary Library, Houston: Swanson Analysis Systems Inc.; 1992.
- “Slab Superstructure Details Standard Details”, Structural Standards Manual, Maryland Department of Transportation State Highway Administration Office of Bridge Development, March, 2006

- Huckelbridge Jr, Arthur A, Hassan El-Esnawi, and Fred Moses. "Shear Key Performance in Multibeam Box Girder Bridges." Journal of Performance of Constructed Facilities. 9. 4 (1995): 271.
- Miller, R. A., G. M. Hlavacs, T. Long, and A. Greuel. "Full-Scale Testing of Shear Keys for Adjacent Box Girder Bridges." PCI JOURNAL. 44 (1999): 80-91.
- Lall, J., S. Alampalli, and E. F. DiCocco. "Performance of Full-Depth Shear Keys in Adjacent Prestressed Box Beam Bridges." PCI JOURNAL. 43. 2 (1998): 72-79.
- Badwan, Inmar Z, and Robert Y Liang. "Performance Evaluation of Precast Posttensioned Concrete Multibeam Deck." Journal of Performance of Constructed Facilities. 21. 5 (2007): 368.
- Wolanski, Anthony J. Flexural Behavior of Reinforced and Prestressed Concrete Beams Using Finite Element Analysis. Thesis (M.S.)--Marquette University, 2004, 2004.